NOTICE

CERTAIN DATA CONTAINED IN THIS DOCUMENT MAY BE DIFFICULT TO READ IN MICROFICHE PRODUCTS.

Appendix V

DOE/ER/40518--T1

DE91 007404

An Expression of Interest

In a

Super Fixed Target Beauty Facility (SFT)

at the

Superconducting Super Collider

(May 25, 1990)

AS05-89ER40518

DISCLAIMER

This report was prepared as an account of work sponsored by an agency of the United States Government. Neither the United States Government nor any agency thereof, nor any of their employees, makes any warranty, express or implied, or assumes any legal liability or responsibility for the accuracy, completeness, or usefulness of any information, apparatus, product, or process disclosed, or represents that its use would not infringe privately owned rights. Reference herein to any specific commercial product, process, or service by trade name, trademark, manufacturer, or otherwise does not necessarily constitute or imply its endorsement, recommendation, or favoring by the United States Government or any agency thereof. The views and opinions of authors expressed herein do not necessarily state or reflect those of the United States Government or any agency thereof.

MASTER

DISTRIBUTION OF THIS DOCUMENT IS UNLIMITED

Abstract

The concept of a Super Fixed Target Beauty Facility (SFT) which uses a relatively low intensity 20 TeV proton beam as a generator of very high momenta B's is an exciting prospect which is very competitive with other B factory ideas. The yields of B's in such a facility are quite high ($3x10^{10}$->10^{11} B's per year). At this level of statistics, CP violation measurements will be possible in many modes. In addition, the fixed target configuration, because of the high momenta of the produced B's and the resulting long decay lengths, facilitates the detection and reconstruction of B's and offers unique opportunities for observation of the B decays. The limited solid angle coverage required for the fixed target spectrometer makes the cost of the facility much cheaper than other e^+e^- or hadron collider options under consideration.

The relatively low intensity 20 TeV beam (1->$2x10^8$ protons/second) needed for the SFT makes it possible to consider an extraction system which operates concurrently and in a non-interfering manner with the other collider experiments. One possible method for generating such a beam, crystal channeling, is discussed.

Parties to the SFT EOI

University of Athens:	S.E. Anassontzis, S. Katsenevas, C. Kourkoumelis, P. Ioannu, G. Kalkanis, T. Premantiotis, A. Manousakis-Kaftsikakis, L.K. Resvanis, P. Spentzouris, G. Voulgaris
Bratislava University:	B. Sitar, S. Tokar
Univ. of Cal., Berkeley:	H.C. Ballach, H. Bingham, J. Lys
Univ. of Cal. , Los Angeles:	A. Boden, D. Cline, J. Rhoades
Carnegie Mellon:	J. Russ
Duke University:	L. Fortney, W. Kowald
Dubna:	J.A. Budagov, N.S. Angelov, A.G. Asmolov, N.I. Chernov, I.N. Churin, I. E. Chirikov-Zorin, J.I. Davidov, V.H. Dodohov, A. T. Filippov, V.B. Flyagin, V.V Glagolev, V.M. Grebeniuk, V.V. Ivanov, B.A. Khachaturov, D.M. Khazins, S.M. Korenchenko, S.N. Maliukov, V.I. Moroz, G.A. Ososkov, N.O. Poroshin, V.I. Prihod'ko, S.I. Merzliakov, N. A. Russakovich, G. G. Takhtamyshev, A.G. Volodko, ; E.N. Tsyganov, S.V. Borodin, Y.N. Gotra, V.N.Pozdnjakov, V.N. Ryzkov, A.B. Sadovsky, A.M. Taratin, V.G. Timofeev, S.A. Zaporozhets
Erevan State University:	S.L. Bagdasarov, G.S. Pogosian
Fermilab:	R. Carrigan, D. Christian, M. Haire, P.O. Mazur, C.T. Murphy, S. Peggs, S. Pruss, R.P.Smith, L. Spiegel
University of Houston:	G. Mo, K. Lau
Gomel State University:	A.M. Dvornik, N.V. Maksimenko
Inst. of Exp. Physics, Kosice:	E. Kladiva, J. Nemchik, L. Sandor
Lebedev Physical Institute:	B. Govorkov, L.N. Shtarkov, G. Sokol
University of Lecce and INFN:	P.Creti, E. Gorini, F. Grancagnolo, M. Panareo, O. Palamara, F. Palama, P. Pistilli
Leningrad Institute:	A. Khanzadeev, V. Samsonov
Los Alamos National Laboratory:	P.L. McGaughey
Northwestern University:	M. Block, M. Recagni
Inst. of Phys, Belorussian Acad. of Sc.	A.S. Kurilin, V.S. Rumiantsev
McGill University:	J. Trischuk
Univ. of New Mexico:	J. Ellison
Oak Ridge National Lab:	H. Brashear, N. Ericison, T. Gabriel, T. Moore
Nanjing University:	T.Y. Chen, N.Yao
Northern Illinois Univ.:	D. Kaplan

Univ. of Pavia and INFN:	L. Antoniazzi, G. Boca, M. Cambiaghi, G. Introzzi, G. Liguori, S. Ratti, P. Torre
Univ. of Pennsylvania:	W. Kononenko, W. Selove
Shandong University:	M. He, N.J. Zhang, C.R. Wang, Z.L. Cao, C. Wei, B.T. Zou
Univ. of South Alabama:	K. Clark, M. Jenkins
Univ. of South Carolina:	F. Avignone, R. Childers, C. Darden
State Univ. of New York, Suny:	C.R. Sun
Inst. of HEP of Tbilisi Univ.	G.A. Chlachidze, D.Q. Djincharadze, I.A. Minashvili,M.S. Nioradze, Z.R. Salukvadze,
Sofia University	L. Litov
SSC Laboratory:	J. Kuzminski, T. Toohig
Univ. of Texas, Austin:	B. Newberger
University of Wisconsin:	A. Erwin, M.A. Thompson
Vanier College:	M. Cooper
Univ. of Virginia:	M. Arenton, S. Conetti, B. Cox, C. Dukes, A. McManus, K. Nelson

Contact: B. Cox

High Energy Physics Building
C/O J. W. Beams Laboratory
Dept. Of Physics, Univ. of Virginia
McCormick Rd., Charlottesville, Va 22901

BITNET: Cox@FNAL
DECNET: UVAHEP::COX
FAX: 804-924-4576

Alternative Contacts: S. Conetti

High Energy Physics Building
C/O J. W. Beams Laboratory
Dept. Of Physics, Univ. of Virginia
McCormick Rd., Charlottesville, Va 22901

BITNET: Sergio@FNAL
DECNET: UVAHEP::SERGIOI
FAX: 804-924-4576

C.T. Murphy

MS 357 , Fermilab
PO 500, Batavia, Il. 60510

BITNET: Thornton@FNAL
DECNET: FNAL::Thornton
FAX: 708-840-4343

Table of Contents

I. Physics Goals and Technical Advantages of the SFT Facility

The 20 TeV Super Fixed Target B Physics Facility (SFT) contains two major components, the crystal channeling extraction/proton beam transport system (Figs. 1,2,3) and the fixed target beauty spectrometer (Fig. 4). This Expression of Interest describes the motivation for pursuing B physics in this manner and contains a conceptual description of the components of the SFT facility. We have considered two general approaches for the SFT spectrometer: open geometry and restrictive geometry. Open geometry gives large acceptance for a wide variety of decay modes and gives the opportunity of tagging by observation of the second B decay in the event. However, the detector must deal with the full interaction rate. Restrictive geometry spectrometers emphasize rare low multiplicity decays such as $B \rightarrow \pi^+\pi^-$ and minimize rates in the detectors per interaction. This type of spectrometer offers simplicity of triggering and cleanliness of event reconstruction. Both approaches seem promising for a 20 TeV fixed target facility. In the sections that follow, we limit ourselves to the open geometry spectrometer which is the more general approach. We describe the physics potential of a 20 TeV open geometry fixed target experimental facility for doing beauty physics, describe the preliminary designs for the components, and give a cost estimate based on a preliminary model for various aspects of the extraction system, beam transport and spectrometer. In many cases there are alternative choices for technologies that must be investigated and compared with the ones described in this document before final choices can be made.

While there are many areas of physics that can be explored by a 20 TeV Fixed Target facility such as that described below, the major impetus for the SFT is beauty physics. The study of the B system is of fundamental importance[1] and has been a major area of activity, involving a considerable segment of the high energy physics community in the past few years. The possibility of an extracted 20 TeV SSC beam offers an exciting opportunity to address all the physics issues presently thought to be important in B decay in a fixed target experimental configuration. This configuration is relatively well understood, tractable and economical to prepare compared to that of the hadron collider, and offers the potential of producing a much greater number of reconstructable B's than can be obtained by any other method.

Among the topics that can be addressed with the large B statistics obtainable in the SFT are:

1. The measurement of the production of the heavy B quark and the attendant fragmentation and hadronization into the various B hadron species B_u, B_d and B_s.

2. The measurement of the lifetimes of the various species.

3. The determination of branching ratios for various decay modes.

4. The determination of the mixing of particle and antiparticle.

5. The observation of rare decay modes.

6. The detection and precision measurement of CP violation effects.

While some of these topics will be explored at other B facilities between now and the beginning of physics research at the SSC, studies of most rare decay modes and CP violation require very large statistics[2] and, almost certainly, will require the large B decay data samples achievable at the SSC for precision measurements.

To obtain an estimate of the pN→BB production cross section at $\sqrt{s}$ =193 GeV, we have used the third order (in α_s) calculations of K. Ellis et al[3] which predicts 2.5 to 10 μb total beauty cross section. Note that this cross section for beauty at the SFT is of order of the charm cross section at present Fermilab fixed target energies. Since we plan to use Be foils interspersed with the silicon measurement planes of the SFT silicon microvertex detector as a target, we must determine the pSi and pBe beauty and total cross sections. Assuming the heavy flavor production increases with atomic number of the target like A^1, the beauty production cross section for pBe will be between 23 and 90 μb and for pSi between 70 and 280 μb. Taking the total inelastic pN cross section at $\sqrt{s}$ =193 GeV to be 38 mb and assuming an A dependence of $A^{0.72}$, we obtain pBe and pSi total cross sections of approximately 185 mb and 420 mb respectively. Therefore, taking into account the relative amounts of Be and Si in the microvertex detector target section (0.063λ of Be and 0.013λ Si), we estimate that between 1/1900 and 1/7700 of $\sqrt{s}$ =193 GeV interactions initiated in the target section will contain a $B\bar{B}$.

While this ratio for $\sqrt{s}$ =193 GeV pSi interactions is not as great as that expected in the hadron collider configuration (1/500-1/200), there are aspects of the fixed target configuration which can lead to a greater fraction of the produced B's actually written to tape and eventually reconstructed. In addition the fixed target configuration offers the unique opportunity of directly observing and measuring some significant fraction of the B's, an option that is available in no other experimental configuration. Thus, the factor of approximately 10 difference in the yield per interaction between the SSC collider and the SSC fixed target mode becomes much less significant when the unique features, relative simplicity and relative economy of the fixed target experiment are compared to the formidable challenges and expense of attempting a comparable B collider experiment.

One of the main points in favor of a fixed target configuration is the much higher momenta of the B's produced in the SSC fixed target interactions compared to those produced in the SSC collider configuration. There are several technical advantages which arise from this high momentum. The high momentum produces very long average decay lengths resulting in the unique situation (among all the options for doing B physics) where B's can pass through many microvertex planes before decaying. In SSC fixed target interactions, an average B will travel 9.5 cm before decaying (see Fig. 5 for a typical event and Fig. 6a and and 6b for the longitudinal and transverse decay distributions respectively for $\sqrt{s}$=193 GeV B production and decay) and, as discussed in Section III.B, pass through approximately 15 silicon planes in the SFT microvertex detector. This allows the possibility of directly observing the B in these spectacular events, and determining whether it is neutral or

charged (B_u or $B_{d,s}$). Furthermore, if a magnetic field is imposed on the silicon microvertex detector (an option under discussion), the sign of the charge of the B_u can be determined for a significant fraction of the B_u's. Particle/antiparticle tagging is critical to CP violation measurements but is difficult in other experimental configurations because of the difficulty in determining the charge of the B's from reconstruction of all their secondary decay products. There will be a relatively high probability of missing or adding a track in reconstructing the B vertex. Both the direct observation of the B tracks and the prospect of having track information between the B decay vertex and the primary production vertex enhance greatly the probability of determining correctly the charge of the B either through direct observation or by determination of the charge via reconstruction of secondaries. This improves tagging. For example, in the $B\rightarrow\mu$ trigger sample discussed in Section IV.D, the charge of the muon, which is ambiguous because of the mixing of the B's or the $B\rightarrow D\rightarrow\mu$ decay process, need not be used as a tag. Observation of the charge of the parent B will replace the muon charge as the tag in the case of the $B_u\rightarrow\mu$ decays.

Another advantage of the higher momenta of the fixed target configuration is the better track resolution due to the smaller multiple scattering of B decay secondaries (roughly half the resolution error even in the relatively high energy Fermilab fixed target environment). While it is true that the Lorentz expansion of the decay length is compensated for by the decrease in the average angle of secondaries from B decay such that the impact parameters of these secondaries remain of the same order of magnitude independent of the total center of C>M energy, the multiple scattering of the B decay products becomes almost completely negligible in 20 TeV interactions. Thus, the ability to resolve secondary vertices improves. In addition, the negligible multiple scattering in Lorentz boosted 20 TeV events allows the use of more measurement planes leading to the opportunity mentioned above of directly observing B's.

Higher momentum of the B's also makes possible tractable trigger strategies (in particular trigger strategies based on leptons). For example, muon triggers which depend on the separation of muons from hadrons become difficult if the muon momentum is too low (a muon shield cannot be made thick enough to range out hadrons effectively). As demonstrated in various studies[4], the muon momentum is low for producing a single muon trigger capable of collecting a large fraction of the B muonic decays in SSC collider events. No such problem exists in the SSC fixed target configuration where the mean and median lepton momenta are 280 GeV/c and 120 GeV/c respectively. The large lepton momentum also helps if an electron trigger is contemplated since distinguishing an electron from a hadron becomes progressively easier for both TRD's and calorimetry as the energy of the electron increases. These more powerful triggers have the advantage of minimizing the required data acquisition systems or on-line microprocessor farms, and the sometimes ignored advantage of reducing enormously the off-line computing load.

Another aspect of fixed target events which makes detection and reconstruction of B's easier is the relatively low multiplicity of the events. At $\sqrt{s}$=193 GeV the average event is expected to contain approximately 23 charged tracks and 10 π^0's. This is to be compared with an anticipated multiplicity of a few hundred in a $\sqrt{s}$ = 40 TeV pp collision. In addition, the B events themselves, at $\sqrt{s}$ = 193 GeV, have approximately the same low

multiplicity (an average of 24 charged tracks). This low multiplicity greatly simplifies beauty triggers based on the hadronic characteristics of B events, as well as off-line reconstruction of B events.

The detector components of the SFT themselves can be arranged in a simpler and more economical and effective way than the collider counterparts, even using today's technologies. In particular, the silicon microvertex detector (Fig. 8) can be a simple, planar arrangement leading to economies of effort and money in construction. The detector as discussed in Section III.B can be arranged so that the B decays occur inside the detector at most 6 mm before a measurement plane, leading to excellent vertex resolution.

Finally, there is the obvious advantage that the size of a fixed target beauty experiment is very modest because of the small solid angle that must be covered to capture the B decay products. As will be discussed in subsequent sections, the SFT spectrometer is designed to cover the 3 ->75 mrad forward cone. With this coverage, approximately 70% of all $\overline{B}$'s will have their decay products within the geometric acceptance of the spectrometer at $\sqrt{s}$=193 GeV. If we require that both B's in a given event have all decay products in the acceptance of the spectrometer, a geometric acceptance of 45% is obtained.

In summary, the large numbers of B events produced in $\sqrt{s}$ =193 GeV/c interactions plus the technical advantages of the fixed target option (compared to SSC collider 40 TeV interactions) and the experience that will be accrued in the next few years in similar fixed target configurations at Fermilab make the idea of an SSC fixed target B experiment very attractive. In Table I we summarize and compare the important global aspects of the various beauty hadroproduction options. In Section IV.D, it will be shown that the yields of B's possible using the SFT are more than adequate (indeed, by one to two orders of magnitude) to detect at the 3σ level a CP violating asymmetry of 15% in the $B \rightarrow J/\Psi K^0_S$ decay mode, just one of many exclusive modes that are expected to exhibit CP violation effects. Our detailed analysis of just this one decay mode agrees with more global studies[6] showing that experiments producing 10^9 B's can make precise CP measurements. Thus, with the estimated production of 3×10^{10} ->10^{11} B's per year for the SFT, we expect to be able to study CP violating effects with good statistics in many decay modes.

Table I

Important Parameters of Beauty Production
in Various Hadronic Experimental Configurations

	TeV II Fixed Tgt	TeV I Collider	SSC Collider	SSC Fixed Tgt
Int Rate	10^7-10^8/sec	10^5/sec*	10^7/sec**	10^7/sec
$\sigma(pN \rightarrow B\bar{B})$	10 nb	20 μb	200-500 μb	2.5 -10 μb
$B\bar{B}/10^7$ sec	10^7-10^8	$4x10^8$	$2x10^{11}$-$5x10^{11}$	$1x10^{10}$-$5x10^{10}$
$\sigma(B\bar{B})/\sigma_T$***	1/1250000	1/2500	1/500-1/200	1/7700-1/1900
Multiplicity	≈15	≈45	"few" hundred	≈20
$\langle p_b \rangle$	143 Gev/c	38 GeV/c	51 GeV/c	635 GeV/c
$\langle p_B \rangle$	118 GeV/c	22 GeV/c	43 GeV/c	445 GeV/c
$\langle p_\mu \rangle$	32 GeV/c	13 GeV/c	36 GeV/c	280 GeV/c
Median B Decay Length	8mm	1.5mm	3mm	42mm
Mean B Decay Length	16mm	4.7mm	13mm	95mm

* Present luminosity ≈ 10^{30} cm^2 s^{-1} for the Fermilab Collider. Presuming the injector upgrades and corresponding detector upgrades to take advantage of the higher luminosity, this may be increased to $5x10^{31}$ cm^2 s^{-1}.

** 10^7 interactions per second is taken as a limit for a high rate 4π B physics collider detector to avoid the problem of multiple high multiplicity events per bucket.

*** Taking into account the atomic number enhancement of the heavy flavor cross sections in heavy targets relative to the total cross section.

II. Conceptual Design of the 20 TeV Extracted Proton Beam

The idea of using a 20 TeV proton beam from the SSC as a generator of B events has great technical and financial merit. It is desirable for such a beam to run concurrently and in a non-interfering way with the collider program. In addition, taking as a criterion that the SFT must use no more beam than a high luminosity intersection region (which at $L=10^{33}$ cm^2s^{-1} uses 10^8 protons per second from each beam), the desired SFT proton beam will have an intensity of $1->2x10^8$ protons per second. This, as shown below, will generate 10^7 interactions per second in the SFT microvertex target. Among the possibilities for slow extraction of this low intensity proton beam is crystal channeling[7]. This technique is well matched to the desired SFT beam intensity and appears to be a viable option for producing a non-interfering extraction system.

There are two technical issues which impact on the feasibility of this type of extraction. One is the efficiency of the channeling process itself. Any evaluation of the channeling must include the effects of the crystal curvature which is an integral part of the extraction process. The other issue is the method of bringing a small part ($1-2x10^8$ protons per second) of the circulating beam (few $x10^{17}$ protons per second) to bear on the crystal in the proper manner. In the following two sections, these issues are discussed in more detail.

II.A Crystal Channeling

First proposed by Stark in 1912 and then observed experimentally in the mid 60's, the channeling of charged particles in crystalline solids has by now reached a level of some maturity. Moreover, the possibility of interesting effects and novel applications of the channeling of high energy particles has stimulated research at relativistic energies[8]. In some respects, the theory of channeling of relativistic particles is simpler than that of channeling of low energy particles. The possibility of steering a beam of charged particles by channeling them in a bent crystal was first suggested by Tsyganov[9] in 1976. Since that time, this effect has been demonstrated experimentally at several laboratories[10]. Bent crystals have been used as optical elements in an external beam line at Fermilab[11], and beam extraction has been performed at Dubna and Serpukhov[12] using crystal channeling.

The physics of bent crystal channeling at relativistic energies is reasonably well understood theoretically. There are essentially three ways that a particle incident on a crystal is dechanneled: by multiple scattering, by crystal curvature (actually a reduction of the effective channel potential by the centrifugal force), and by the surface acceptance of the crystal channel[13]. Many theories of multiple scattering have been constructed, and the reduction of the phase space of the channeled particles due to the centrifugal potential as a function of the bend angle has been obtained by Ellison[14] and Kudo[15]. Theories including both multiple scattering and bending dechanneling have recently been developed[16]. The surface acceptance dechanneling is independent of the other two dechanneling effects. It simply reflects the facts that the low order atomic planes which provide the channeling

force occupy some fraction of the crystal volume, and that any real beam contains a distribution of transverse energy, and that some fraction of particles will have transverse energy which exceeds the channel well depth. For a given distribution, the intuitive expectation for the channel acceptance can be shown to follow from the Fokker-Planck transport calculation of the dechanneling in the limit of zero depth[17]. While the qualitative agreement between theory and experiment is reasonable, some quantitative differences in the dechanneling remain. As the interest in using crystals as optical elements in accelerators and in other applications grows and, in particular, the issue of slow extraction at the SSC is addressed, this research should continue to be pursued. While understanding these differences is important for the interpretation of experiments in the 10-500 GeV range, the uncertainties in the predictions at 20 TeV are less substantial. Channeling in bent crystals at 20 TeV can be described reasonably well by these calculations, especially as it pertains to extraction at the SSC.

There are four key points which make channeling extraction at the SSC feasible and predictable. First, the bend angle required is rather modest (about 100 μrad) and can be accomplished reasonably easily even for 20 TeV protons. For a bend angle of such a size, the bending dechanneling is not particularly serious in any of the models considered. It should be less than 10% (see Fig. 7) even for rather short crystals such as the 3 cm silicon crystal which we plan to use in the SFT extraction system. Bending dechanneling increases as crystal length decreases, but the radius of curvature necessary for the extraction system described below is so large that this does not cause a problem.

Second, the multiple scattering contribution to dechanneling is also small at 20 TeV/c. This is a consequence of the rapid decrease in the scattering coefficient with increase in the projectile momnetum. The fact that we require only a short crystal to obtain the requisite bending (without incurring unacceptable bending dechanneling) also helps. Multiple scattering dechanneling should be less than 4%.

Third, the surface acceptance dechanneling loss mechanism, while dominant, is still not large enough to be serious. The magnitude of this loss mechanism is due to a geometric contribution and to an angular acceptance effect. The geometric contribution is fixed by the choice of silicon as the crystal material. This geometric dechanneling arises from the fact that the atoms of the crystal plane subtend a fraction of the cross sectional area of the crystal face. This fraction is approximately 20% for the silicon (110) plane. However, this 20% of the surface area is not opaque to 20 TeV protons as discussed in the next paragraph. The other contribution to surface dechanneling is due to the overlap of the transverse momentum phase space of the incident beam with the channel width. The magnitude of the overlap is set by the width of the transverse momentum distribution and the depth of the potential for the channel. The measure of this overlap is the critical channeling angle above which a particle will not be captured. For 20 TeV protons in the (110) planes of Si, this angle is about 1 μrad. Crystals of the high quality necessary to meet this specification are available. For a given distribution of angles in the beam intercepting the crystal, it is a good approximation to assume that all tracks with angles greater than the critical angle of 1 μrad will not be channeled. To determine this fraction for a real extraction scheme requires some knowledge of the phase space distributions of the particles

incident on the crystal. Assuming that $\beta \approx$ 0.5 km in the East Utility straight section of the SSC and that the large amplitude portion of the circulating beam has approximately the same emittance as the central core of the circulating beam, we calculate from the SSC normalized emittance[18] of π mm mrad, an angular divergence $\sigma \approx$ 0.3 μradians. Assuming a Gaussian distribution, the angular acceptance is essentially 99% of the incident beam, making dechanneling due to this source negligible.

The final factor that makes channeling feasible is the possibility that protons which dechanneled on the first pass through the material will channel on subsequent passes of the beam through the crystal. Dechanneled protons will pass through the crystal with a small fraction of them suffering the usual nuclear interactions due to the material that they traverse after dechanneling takes place. Therefore, most of the dechanneled protons survive the crystal (only 3% interact on average) even if they are not channeled. In a recirculating machine, the surviving protons can be channeled on subsequent passes.

To summarize, we expect the major source of dechanneling to be the geometric component of the surface dechanneling (at the 20% level) followed by bending dechanneling (at approximately 10% level). The multiple scattering dechanneling will be less than 4% and the angular acceptance dechanneling is negligible. This leads to an estimate of at least a 65% efficiency for channeling the incident beam at 20 TeV for a single pass. A particle which is dechanneled (or rather not channeled) on a given pass does not necessarily interact in the crystal. The crystal looks like an amorphous material to the dechanneled particle and the particle undergoes normal pSi interactions. Since the crystal is thin (total thickness 6.6% of an interaction length), beam particles make multiple transits through the crystal. Simulations[19] suggest that better than 85% of the flux incident on the crystal can be deflected into the extraction line, taking into account multiple passes. Furthermore, very few interactions of the 2×10^8 incident protons/sec will take place. We expect that for 2×10^8 protons/s incident on the crystal only a few x 10^6 protons/s will interact.

II.B The Extraction Technique

To effect extraction of 10^8 protons/s of the SSC circulating 10^{14} proton beam, a nominal 3mm x 3mm x 3cm silicon crystal will be positioned in the median plane of the SSC approximately five sigma from the central orbit of the beam, where it can intercept 1->2×10^8 protons/s. Since the dechanneled fraction of the incident beam is expected to be approximately 10%-30%, a small portion (approximately 3%) of which will interact, we expect the crystal to produce at most a few x 10^6 interactions per second in comparison to 10^8 interactions per second produced by the collider interaction regions. The remainin unchanneled beam will be transmitted and may be channeled on subsequent passes. Thus the extraction of 10^8 protons/second will use the same number of protons as a high luminosity interaction region and produce only a few $\times 10^6$ interactions/second.

An even more proton conserving mode of operation of the extracted beam would be to use the large amplitude halo. At the interaction points (IRs), quasi-elastic scattering will form an in-aperture, forward peaked halo which will either be lost in regions of high dispersion in the lattice or will be attenuated using collimators in order to minimize

background at the IRs. At SSC beam intensities, the number of these large amplitude particles may be sufficient to make their flux interesting as a source of low intensity proton beam for the SFT. Because they must be disposed of in any case, it is appropriate to consider schemes to manipulate them onto an extraction channeling crystal system, rather than onto a collimator, to make them available for the SFT. However, uncertainties in the magnitude and nature of the halo make it unwise to rely on it as the principal source of protons for the 20 TeV extracted beam.

In either case, a small fraction of the 10^{14} circulating proton beam must be moved into the crystal continuously in order for the crystal to perform its function. Several possibilities have been suggested for producing large enough transverse displacements of a small fraction of the circulating protons far into the crystal in a controlled way. Two examples of such techniques are lattice dispersion and resonance scraping.

The presently favored method for producing the required orbit displacements is based on the use of lattice dispersion generated by the bends of the SSC. By introducing suitable magnetic elements in the East Utility straight section, a dispersive section can be constructed in a limited region and then recombined. Because the SSC beam has a momentum spread σ of approximately 5 GeV/c [21], introduction of this dispersive section into the lattice will inject particles into orbits sufficiently displaced at the position of the crystal. to intercept the crystal and be channeled. Achieveable dispersion function in the East utility straight section at the position of the crystal will cause off-momentum particles to undergo sizable displacements (for example, a dispersion of 1 meter will cause a particle with momentum differing by 5 GeV/c from the central momentum of the beam to be displaced by 250 microns) and to move into incidence on the surface of the crystal. This method of moving off momentum particles bears some resemblance to collimation ideas for linear colliders[20].

The resonant scraping process suggested by Collins[21] bears a considerable relationship to slow spill resonance extraction. Sextupole and decapole driven resonances have been considered for application to the SFT extraction problem. From the standpoint of continuous extraction, decapole resonances are preferred, but the sextupole resonances are more straightforward to implement. Correction style elements might, at least in specific cases, be used. However, the issues of non linear dynamics[22] of beams in accelerators together with the resonance extraction itself[23] are complex and, therefore, we consider this method more speculative and difficult.

For either possibility of generating a large amplitude beam, the step size of the displacement of the beam is an issue. This translates into an effective septum width for crystal extraction, as defined by the misalignment angle between the physical surface of the crystal and the crystallographic planes between which the channeling takes place, and the length of the crystal. This has been of some concern but recent results indicate that the fabrication of crystals with small misalignments is feasible. Effective septum widths smaller than a micron do not seem to be unreasonable. Furthermore, the extraction geometry proposed in II.C circumvents this problem altogether, since the crystallographic planes are parallel to the displacements due to dispersion.

Finally, we would expect dispersion suppression systems to be employed in the utility straights as suggested in the conceptual design study[24]. This clearly implies the need for a dispersion cancellation mechanism in the lattice design in the utility straight sections which might be modified to be useful for a crystal extraction system. Making quantitative estimates for the crystal channeling extraction system is complicated by uncertainties in the SSC lattice which is still under design and in which the behavior of the large amplitude orbits is just becoming understood. Conversely, this situation provides an opportunity to build enough flexibility into the system to accommodate the crystal channeling needs. Techniques for beam cleanup (which are presently being suggested for the utility straight sections) will have to be developed, therefore the behavior of the large amplitude portion of the circulating beams must be understood in these sections whether or not a portion of the beam is extracted for the SFT.

II.C The SFT Extraction System

Although the relationship between the lattice and the extraction system is in an early stage of development, we are able to configure a possible system for extraction. The preliminary layout of the design of the SFT extraction system and external beam transport are shown in shown Figs. 2 and 3. The extraction of the 20 TeV beam is initiated in the East utility straight section of the SSC, just south of the East Campus. In Fig. 3c, we show the 3 cm silicon channeling crystal positioned in the bend plane of the counterclockwise circulating proton beam. This crystal must be adjustable remotely so that its crystal axis can be aligned with respect to the circulating proton beam and so that its transverse positioning can be varied. The crystal (nominally 3 mm by 3 mm in transverse size and 3 cm long) is bent so as to supply an effective 100 μrad vertical deflection to the portion of the beam which intercepts the crystal and is channeled. The dispersive section mentioned above is designed so that 1.5×10^8 protons per second are directed into the crystal, with 85% of this flux eventually channeled (taking into account multiple passes), leading to 1.3×10^8 protons/sec deflected into a Lambertson channel.

Approximately 200 meters downstream of the crystal is the second element of the Lambertson dogleg, schematically shown in Fig. 3. The portion of the beam deflected by the crystal is separated by 20 mm at this point from the circulating beam and passes through the field free region in a set of 16 Lambertson magnets, while the circulating beam is bent by 1.4 mrad back into the ring. After traversing the Lambertson magnet system, the channeled 1.3×10^8 protons pass into the external beam transport.

II.D The SFT Beam Transport

The least innovative feature of the SFT is the proton beam transport from the extraction region to the SFT spectrometer. A possible configuration is shown schematically in Fig. 2. As shown, the transport consists mainly of a safety bend of 4 mrad which deflects the extracted beam away from the machine into the SFT. A reverse 4 mrad bend is needed just before the SFT to keep the muon vector from the dumped beam pointed at the M9 monitor hole (see Fig. 1). In addition to the dipoles, a number of targeting quadrupoles will

be needed to focus at the silicon microvertex detector/target. Presumably the magnets for this beam can be culls from the SSC magnet production program since high dipole field quality is not a criterion in this external beam line. Accordingly these magnets are not costed in Section VI. The total length of the beam transport from the crystal extraction point to the silicon microvertex target of the SFT is approximately 3000 meters.

II.E The SFT Experimental Area

The Super Fixed Target Experimental area is positioned approximately 100 meters from the SSC tunnel (as shown in Fig. 2) and is approximately 200 feet underground at the level of the SSC beam. The horizontal displacement of the area from the beam is adequate to avoid the muon halos associated with the circulating beams. The enclosure required for the SFT spectrometer is 100 meters in length and 20 meters wide. The overhead clearance needed for equipment movement is 10 meters and the beam is 5 meters above the floor. Access is provided to this area via a displaced drop hatch some 20 meters to the east of the upstream end of the hall. The SFT spectrometer as shown in Fig. 4 will fit in the experimental hall with some space reserved for a work area at the 200 ft. level.

Personnel access to the experimental area while the collider is operating is desirable. Estimated radiation levels are low enough to permit access, provided the crystal extracted 20 TeV beam is properly interlocked. Beam stops and removal of the crystal are possible requirements for access.

The plan for the East Campus footprint is shown in Fig. 1. The East Campus, as presently envisioned, is large enough to accommodate the SFT experimental hall within its above ground boundaries (solid lines) without further acquisition of surface area. The profile of the underground acquisition (dotted lines) is adequate to contain the muon vector from the extracted proton beam.

III. The Super Fixed Target Beauty Spectrometer (SFT)

The very important experimental advantages that an SSC fixed target configuration offers must be capitalized on by the design of the SFT spectrometer. The SFT spectrometer (Fig. 4) is aimed at taking advantage of the following:

1. Long B decay lengths to make direct observations of the B's and to facilitate better tagging.

2. High momentum of the B's and their decay products in the design of the silicon microvertex detector to make higher resolution measurements of the secondary vertices.

3. High momentum of the B's to design efficient, relatively simple triggers which can collect data samples rich in B events.

4. Limited solid angle coverage required to capture all B decay products from both B's in a significant fraction of the events.

A significant feature of the plan for implementing the design of this spectrometer is the existence of the ongoing fixed target program of heavy flavor physics at Fermilab. The similarity of the technical challenges in the Fermilab program to those that must be faced at an SSC Fixed Target Beauty Facility insures that most of the serious issues have already been or will soon be addressed in real and, (because of the much lower cross sections at Fermilab energies), more difficult experiments. For example, the requirements of dealing with the 16.7 ns separation of proton bunches at the SSC is being addressed in a number of Fermilab experiments which have to handle the 18.7 ns bunch structure. A second example is the ongoing work in several experiments with interaction rates of 10^7/s.

A second significant feature of the SSC fixed target configuration is the relatively low cost (as detailed in Section VI) of a 20 TeV fixed target spectrometer adequate to address the full range of B physics issues as compared to a collider detector. Even ignoring relative costs, collider detectors may not be able to address the B physics issues as well as the fixed target spectrometer because of the technical difficulties.

A third significant feature of the SFT is the relatively small advance in technology needed to implement the SFT detector. Indeed, existing technologies available in 1990 are almost sufficient to construct the SFT as outlined below. While this spectrometer would quite naturally be assembled using the most up to date technology available at the time of construction of the various components, a very respectable facsimile of it could be prepared with present day technology Any additional tecjhnical developments required can be immediately checked in the Fermilab fixed target experiments.

The original model for the SFT spectrometer was developed in August, 1989 at the Breckenridge meeting[5]. This "ideal" fixed target hadron beam spectrometer incorporated some of the best features of many of the "open geometry" fixed target spectrometers

presently operating at Fermilab. Ideas from that meeting have been developed further at the 20 TeV Fixed Target Beauty Facility Workshop at Fermilab in November of 1989 and in other meetings. The resulting spectrometer ideas have been incorporated in the SFT spectrometer which we describe below. Several of the choices of technologies have been left open, in anticipation that the results of the next two runs of the Fermilab program and the generic and subsystem R&D program initiated by the SSC will indicate the best options.

As shown in Fig. 4, the SFT spectrometer is 70 meters long and 10 meters wide at its downstream end. The various components of the SFT include two large analysis magnets, a silicon microvertex detector, several stations of PWC wire and pad chambers, a RICH detector, an electromagnetic detector and a muon detector. Optional items under discussion but not shown in Fig. 4 are a 60 kG microvertex detector magnet which is under study for B_U tagging, and the use of silicon planes distributed along the beam to help extend the coverage to smaller angles. The following sections describe schematically these individual components.

III.A Analysis Magnets and Magnetic Field Configuration

The SFT has two large aperture analysis magnets as shown in Fig. 4. The present design of the SFT calls for these magnets to be run with equal and opposite polarities to preserve initial angles in both bend and non-bend planes, simplifying trigger strategies and with the intent of minimizing the spectrometer transverse size. Momentum resolution comparable to present Fermilab fixed target spectrometers has been achieved in the SFT by increasing the overall length of the spectrometer, rather than by increasing the $\int B \cdot dl$ of the magnet system or attempting to achieve exceptional chamber resolutions. We take advantage of the SFT silicon microvertex detector, which allows very precise front track measurements, to shorten the upstream section of the spectrometer and, thereby, minimize magnet apertures.

Lengthening the SFT spectrometer to obtain good momentum resolution on high energy tracks for 20 TeV interactions does not appreciably increase the size of the various SFT spectrometer elements relative to those of present day Fermilab fixed target spectrometers, since the average angle of the Lorentz boosted secondaries decreases by approximately 1/3 in going from Fermilab fixed target energies to the SSC fixed target energies. The percentage of events from various B decay modes (such as $B \rightarrow De\nu$, $B \rightarrow K\pi$, $B \rightarrow J/\Psi K \rightarrow \mu\mu K$, $B \rightarrow J/\Psi K\pi \rightarrow \mu\mu K\pi$, etc) in which all the secondaries from one of the B's are in a 3->75 mrad cone is 70%. The fraction for which all secondaries from both B's are in the 3->75 mrad cone is 45%. So one can see that the solid angle coverage need not be large to capture large fractions of all B decays, a critical consideration in minimizing cost.

The spectrometer magnet placements, at 11 and 22 meters from the target respectively, are provisionally chosen to obtain good momentum resolution and acceptance. The p_t kick of both magnets is chosen to be 1 GeV/c, which will achieve 20-30 MeV/c^2 mass resolution for the reconstructed B. Positioning the magnets at these locations dictates the apertures to be 1.8 meters vertical x 2.0 meters horizontal for M1, and 3.3 meters vertical x 3.5 meters horizontal for M2. The physical length of each magnet is 2.25

meters, and we require an $\int B \cdot dl \approx 33.33$ kG-m.

We have investigated superconducting and conventional versions of M1 and M2 which satisfy our requirements. The parameters of these magnets are given in Table II below:

Table II

SFT
Conventional and Superconducting
Analysis Magnet Comparison

	M1		M2	
	Conventional	Super	Conventional	Super
Iron [lbs]	1.0×10^6	4.5×10^5	2.3×10^6	1.4×10^6
Conductor[lbs]	3.0×10^5	1.4×10^4	7.8×10^5	2.8×10^4
Cryostat [lbs]	-	2.0×10^4	-	3.0×10^4
Total [lbs]	1.3×10^6	4.8×10^5	3.1×10^6	1.5×10^6
Power [MW]	1.0	0	2.7	0
Stored Energy [MJ]	7.3	7.3	23.3	23.3
NI [Amp turns]	2.1×10^6	2.1×10^6	4.0×10^6	4.0×10^6
I [Amps]	5000	5000	5000	5000
Turns	420	420	800	800
Conductor Len [ft]	2.0×10^4	1.6×10^4	5.2×10^4	4.5×10^4
Iron Cost	$ 400K	$ 180K	$ 920K	$ 560K
Conductor	$ 600K	$ 80K	$1600K	$ 230K
Labor	$ 150K	$ 200K	$ 370K	$ 400K
Fixtures	$ 60K	$ 50K	$ 120K	$ 100K
Cryostat	-	$ 500K	$ -	$ 800K
Total Cost	$1210K	$1010K	$3010K	$2090K

The preliminary costs in Table II would point to a choice of the superconducting option for both magnets, except for the availability to the SFT collaboration of low cost conventional magnet production facilities at JINR, Dubna.

III.B Microvertex Detector

The configuration of the SFT microvertex detector is similar to the planar silicon microvertex detectors in operation in several Fermilab fixed target experiments. The SFT microvertex detector will be operated as a semi-live target, with a combination of Be foils and the silicon planes providing the target material for the 20 TeV proton beam. As shown schematically in Fig. 8, the initial "target section" of the SFT microvertex detector consists of 30 planes of 5 cm x 5 cm, 200 micron double sided silicon detectors[25], spaced 6 mm apart, with thirty 850 micron Be foils attached to each plane to increase the interaction

length of each target station. The target region of the detector, therefore, has a total thickness of 7.6% of a nuclear interaction length and 13.6% of a radiation length. The silicon measurement planes in the target section will have strip widths of 25 microns. Because of the very high momentum of the B's ($\langle p_B \rangle$=445 GeV/c), the B decay products have a large momentum, making multiple scattering in the SFT microvertex detector negligible. Even using a 25 micron pitch, the contribution to measurement error due to strip width completely dominates the track error. In contrast, at TeV II a 25 micron strip pitch contributes only one half of the error in the slopes and intercepts of reconstructed tracks. The option of smaller strip size is being considered.

The target region silicon planes will be distributed over a length of 18 cm (one measurement plane approximately every 6 mm). The spacing of the first set of planes is minimized to capitalize on the unique (to the SFT) experimental opportunity of directly observing the B tracks. An B in the SFT with average decay length (9.5 cm) will pass through approximately 15 planes before decaying, taking into account that it will be produced half way, on average, through the target section of the SFT microvertex detector. Simply counting planes would result in a time resolution of approximately 0.1 picosecond for an event with a clear B track.

The "tracking section" downstream of the target region of the microvertex detector will contain 30 additional 200 micron double sided measurement planes distributed over 1.2 meters (one every 4 cm). The second group of silicon detectors is positioned in this extended configuration to provide more lever arm for the measurement of secondaries and to collect more D decays. Because of the very long decay lengths of the B's and D's, it is not unusual to observe D decays an appreciable fraction of a meter downstream of the production target (see Fig. 5 for a typical event). The downstream tracking section is 1.3% of an interaction length and 6.4% X_0, leading to a total microvertex detector thickness of 8.9% of an interaction length and 20% of a radiation length. The double sided planes will be 10 cm x 10 cm and have 50 micron pitch. A few additional pixel planes (200 micron by 200 micron pixel size) may be distributed in the upstream segment to help pattern recognition, provided smart electronics[26] is available to minimize the readout cost of such devices. In both the upstream and downstream sections of the silicon microvertex detector, equal numbers of double sided x/y planes are arranged with 0^0, 30^0, and 60^0 orientations of the x strips with respect to the vertical.

Upstream Segment:	5x5 cm^2 double sided planes/	25 micron pitch (30)	1.2×10^5
Downstream Segment:	10x10 cm^2 double sided planes/	50 micron pitch (30)	1.2×10^5
Total channel count			2.4×10^5

For estimating the cost and number of channels, we ignore the pixel planes until more information can be determined about the cost and style of the readout. The transverse size of the active area of the silicon detector sections is chosen to provide both adequate acceptance for B decay products and to minimize radiation damage. The two extremes, a focussed beam with radius 1 mm or a defocused beam with radius set to match the size and acceptance of the

silicon detector, have been considered for the 20 TeV proton beam. We must either defocus the beam, or operate with a pencil beam and periodically move the detector to spread over a larger area the radiation damage from both the incident protons and the secondaries. The limit for radiation damage is taken to be approximately 10^{14} protons/cm^2 from the test of M. Nakamura et al[27]. This level of reversible damage is anticipated to lead to 20% increase in leakage current and a corresponding degradation in the ratio of average signal to noise in the detector for minimum ionizing particles. Since the silicon microvertex detector presents 7.57% (target region) and 1.31% (tracking region) of an interaction length to the incident beam, the choice of 10^7 interactions per second in the target section as an operating point leads to an incident beam intensity of 1.3×10^8 protons per second passing through the target. In addition to the radiation damage due to the proton beam, the approximately 20 charged secondaries per interaction contribute to the overall radiation damage an amount roughly equal to that caused by the incident beam. In one year of operation we expect the radiation exposure to be approximately 2×10^{14} protons/cm^2.

The expected performance of the microvertex detector has been evaluated using Monte Carlo simulations which include random noise, multiple scattering, gamma conversion, delta ray production and secondary interactions. The track reconstruction efficiency is estimated to be 95%. The resolutions on the found tracks produce vertex resolution in the transverse plane of $\sigma \approx 1.2$ microns and in the longitudinal plane of $\sigma \approx 600$ microns. The tracks themselves are well determined, with x and θ_x residuals of 4.4 microns and 30 μrad respectively. If the criterion for well resolved vertices is set at the 5σ level (ie a separation of primary and secondary vertices of 6 microns in the transverse direction and 6mm in the longitudinal direction), the losses of B's due to confusion of primary and secondary vertices can be minimized. We estimate that over 90% of the B's will survive all vertex cuts.

Readout electronics capable of handling 18.7 ns bucket structure have already been developed at Fermilab[28]. ASIC technology has been used to produce a fast amplifier chip which can operate at high rates and extract the charge from the silicon strips in less than 30 ns. The preliminary results from Fermilab experiment E771 in an 800 GeV/c extracted proton beam indicate a signal duration of under 20 ns with very little noise. The design goal of 20,000 electrons per minimum ionizing particle with 2000 electrons (RMS) of noise has been met on the bench, and the first results under real world beam conditions are encouraging. In addition, a pipelined readout system implemented in FASTBUS is under construction and will be completed in the near future. The task for the future R&D is to see if this system, adequate for the SSC, but constructed with 1980's technology, can be more cheaply constructed for the much larger number of channels required for the SFT live target. Without assuming major decreases in the cost of connectors, cables, boards, and solid state components, it is difficult to anticipate reduction factors of greater than three in the the cost per channel of such a system. Using the real costs of the Fermilab project (approximately $50 per channel for the complete readout chain), we estimate approximately $20 per channel for the equivalent system in 1998, leading to a total cost of approximately $5200K for the electronics. The total cost of the SFT silicon vertex detector is given in section VI.

III.C Charged Particle Tracking System

Since the SFT will operate at rates up to 10^7 interactions per second, and since it is important for complete solid angle coverage to operate as close to the beam as possible, the tracking system has been tailored to correspond to the portion of the solid angle covered. In regions close to the beam, coverage is provided by 6 sets of small wire spacing PWC Chambers(1 mm, 1mm, 2mm, 2mm, 3mm and 3mm respectively) labeled in Fig. 4 as b1->b6 chambers distributed along the beam. The b chambers are desensitized in the beam region ($\sigma \approx 2.25$ cm) and cover out to 20 mrad. In the large angle regions beyond 20 mrad, four sets of straw tube chambers (labeled in Fig. 4 as the c1->c4 chambers) of various radii (4mm, 8mm, 8mm and 16mm respectively) will provide coverage. The c chambers are desensitized in the areas covered by the smaller b chambers. Fast TDC's will be used on the straw tube chambers while a latch system will be used with the small gap PWC's.

The primary device for measurement of tracks in the portion of the spectrometer upstream of M1 is the silicon detector. The purpose of the wire chamber planes (b1, b2 and c1) upstream of the M1 analysis magnet is for measurement of K^0_S and Λ^0 decays. The b3, b4 and c2 chamber sets provide measurements of tracks in the region between the analysis magnets, while b5, b6, c3 and c4 measure the tracks in the section of the spectrometer downstream of M2. Each of the chamber sets b1->b6 and c1->c4 is composed of 8 triplets of 3 planes (x,y and 16.7^0 orientation of the sense wires). The total channel count is 84K for the straw tube chambers and 55K for the PWC's.

In addition to the small gap wire chambers and the straw tube chambers, pad planes are planned for the region downstream of the M2 magnet. These chambers, labeled as p in Fig. 4, will participate in the trigger for the SFT as discussed in Section III.G. The total pad count for these chambers is 24K. The cost of the total system is estimated to be $3165K. Details of this costing are given in Section VI.

III.D π/K/proton Identification System

The strategies for particle identification at the SSC separate into two classes based on the physics topics to be addressed. While searches for new heavy mass particles appear to benefit from simply separating leptons from hadrons, π/K/p separation is crucial for high statistics studies of B physics. The gradual development and even employment of ring imaging Cerenkov counters (RICH) in some experiments (Fermilab E665, for example) point to this as the most complete solution to the problem of π/K/p identification for the SFT. The placement of the RICH in the SFT spectrometer is indicated in Fig. 4.

A schematic of the SFT RICH is shown in Fig. 9a. The radiator vessel is rectangular, of length 16 meters along the beam direction and having a cross section of 8 m in the horizontal and 6 m in the vertical direction in order to accept low momentum (down to 16 GeV/c) trajectories out to 75 mrad. Two large (3.5 m x 5.7 m) segmented mirrors located on the downstream wall of the vessel are tipped slightly to focus ring images onto photodetectors (described below) located outside the experiment aperture, as indicated in Fig. 9a. Beam particles are isolated from the radiator gas by a 2.5 cm radius thin walled

plastic pipe through the center of the vessel. Thus we avoid producing uninteresting rings while retaining a large fraction of the forward rapidity range. Due to the small angular range of the particle trajectories, paraboloid mirror segments may be preferable to spherical segments; however, spherical mirrors will be assumed for the remainder of this discussion.

The operating conditions at the SSC pose challenging conditions on the photodetector component of a RICH. Large interaction rates ($>10^7$/s) in the SFT demand a small dispersion in photoelectron collection times. In addition, a large momentum range for the B decay products (from several GeV/c to >150 GeV/c) is anticipated, so use of a high threshold radiator may be necessary. To demonstrate the required range of coverage, Fig. 10 shows the momentum distribution of π's and K's coming from D's in the decay of $B \rightarrow D\ e\ \nu$. Since the production rate of Cerenkov photons as $\beta \rightarrow 1$ varies quadratically with $1/\gamma_{threshold}$, one requires the most efficient photodetector possible for the high momentum particles.

A solution to these two requirements for the SFT is the recently available technology of multi-anode photomultiplier tubes. The relative simplicity of operation, the reliability, and the speed of response offered by photomultiplier tubes is an attractive alternative to the well known difficulties in the operation of wire chambers filled with TEA or TMAE laden gas mixtures. In contrast to a TMAE gaseous photodetector, the PMT has a very low ($\approx$2 ns) dispersion in photoelectron collection time without the need for elevated temperatures and low pressure[29,30,31]. Alternatively, while TEA may provide an adequately low time dispersion, it is sensitive to photons only in the vacuum ultraviolet region above 7.5eV[32,33]. At these energies the performance of optical components deteriorate rapidly and small amounts (200 ppb) of oxygen contamination in the radiator gas become a severe problem[34]. Since the PMT is sensitive to lower energy Cerenkov photons (2-6 eV) it is much more tolerant of these effects.

A multi-anode photomultiplier will need anode pixel sizes of order a few mm^2 to provide position resolution comparable to that of the alternative photosensitive gas-filled wire chamber equipped with pad readout. Of course, the actual pixel size necessary depends on other factors such as mirror focal length, radiator threshold, momentum range, etc. Resolution finer than the pixel size is possible if the signal is shared among several pixels by analog or digital interpolation methods. The tube envelope is planned to be either hexagonal or square to reduce geometrical inefficiencies when stacking in an array (see Fig. 9b). For a similar reason the sensitive cathode area should be a large (>50%) fraction of the total area of the envelope face. An example of a tube which is almost suitable for this application is the Hamamatsu R2489, shown schematically in Fig. 9c. This photomultiplier has a 7.6 cm square envelope with a sensitive cathode area (6x6 cm^2) covering 62% of the front window area. Although the coarse pixel size of 1.9 cm is larger than desirable, discussions with Hamamatsu indicate that an anode pixel size as small as 2.5 mm square can be achieved in this tube. Further issues under investigation include the efficacy of different amplification structures, e.g. mesh dynodes, crossed wire dynodes, Venetian blind dynodes, microchannel plates, etc, for single photoelectron detection.

An example of how an array of tubes similar to the R2489 might appear in a RICH

photodetector is shown in Fig. 9b. The 7.6 cm square tubes are arrayed at 8 cm pitch to allow for electrostatic and/or magnetic shielding if necessary. The squares in Fig. 9b represent the sensitive area of individual 6 cm x 6 cm photocathodes. An example of relatively fine anode segmentation (8 X 8 pixel array) is indicated in the upper left hand corner PMT. Superimposed on the array are the detected photons produced by a 40 GeV/c pion (γ=280) traversing a 12 m long path in neon gas ($\gamma_{threshold}$=86). Ne is chosen for its relatively high threshold and low chromatic dispersion[35] which may be desirable due to the PMT's large bandwidth. Scintillation photons in Neon are expected to contribute negligible (≤1/track) background due to the small angular acceptance of the optical system. The radiated photons are focused onto the array by a 12 m focal length spherical mirror. The percentage of sensitive area for this photomultiplier array is 56%.

In such a photomultiplier tube array, the gaps between photocathodes are tolerable. We have simulated the SFT RICH photodetector, taking into account geometric losses as well as the statistical generation of photons. For each value of particle γ, Cerenkov rings are centered randomly over a fiducial region of the array. The number of photons generated for each ring is given by

$$N_\gamma = \alpha/\overline{hc} \cdot L_{rad} \cdot \sin^2(\theta_C) \cdot \Delta E$$

These photons are distributed randomly over the ring and are detected by an intercepting photocathode with probability equal to an energy averaged quantum efficiency of a bialkalai photocathode (10%) over a photon energy band ΔE = 4 eV (assuming a UV enhanced glass window).

The expected average number of detected photons, N_{pe}, is given by

$$N_{pe}=N_\gamma \cdot (1/\Delta E) \cdot \int QRT \, dE \cdot \varepsilon$$

where Q is the quantum efficiency, RT is the product of reflection and transmission coefficients of the optical components and ε is a product of other detector efficiencies. For example, the packing fraction of the PMT tubes in the array of Fig. 9b contributes a factor of 0.56 to ε. In the above simulation RT=1, which is approximately true (within 10%) for near visible photons and reasonable quality optics.

A useful figure of merit when comparing different detectors is the quantity N_0, given theoretically by

$$N_0 = (\alpha/hc) \cdot \int QRT \, dE \cdot \varepsilon$$

Experimentally it is calculable through its relation to N_{pe} by

$$\langle N_{pe} \rangle = N_0 L_{rad} \sin^2\theta_c$$

In Fig. 11 the solid lines indicate the expected fraction of Cerenkov rings which are "identified" by the PMT array by requiring more than 5, 8, or 10 detected photon hits per

ring plotted as a function of the γ of the radiating particle. For comparison the predicted ring detection efficiency for a gaseous photodetector using TEA is shown as the dashed curves in Fig. 11. The value of the quality factor N_0=35 for the TEA detector is taken from the results of a E665 RICH prototype reported in ref. 36, while the value N_0=87 given for the PMT is only for comparison purposes. It is calculated by assuming that 0.56 of the total area is sensitive and that the tube has an average quantum efficiency of 10% over a bandwidth of 4 eV.

In addition to detecting a Cerenkov ring, the photodetector must be able to measure its radius with sufficient precision to distinguish between different particle types, e.g. π/K in the context of B physics. In most cases photodetector position resolution dominates the error in radius determination[37]. Thus, the pixel size of the photodetector determines, in a large part, the maximum momentum at which different particle rings may be distinguished. We can examine each of the contributions to errors in the determination of ring radius by remembering that the error in the π light Cerenkov angle is given by

$$(\Delta\theta_\pi)^2 = (\Delta\theta_{Chromatic})^2 + (\Delta\theta_{Geometric})^2 + (s/\sqrt{12}*f)^2$$

where $\Delta\theta_{Chromatic}$ is the error due to chromatic dispersion in the radiator gas, $\Delta\theta_{Geometric}$ is the error due to aberrations, taken to be $0.01 * \theta_\pi$, and $s/\sqrt{12}*f$ is the error resulting from the angular granularity due to pixel size s and focal length f. A smaller error for this last term might be realized by interpolation methods rather than simple digital registration of the photon (pixel) position. At a given momentum,

$$n_\sigma = (\theta_\pi - \theta_K)/\sqrt{(\Delta\theta^2_\pi/N_{pe})}$$

is the number of standard deviations in θ_π separating π and K rings. It is a measure of the probability for incorrectly identifying a π as a K. Once n_σ, $\gamma_{threshold}$ of the radiator gas, the photodetector bandwidth, and the focal length are specified, the pixel size for π/K discrimination at n_σ is given by

$$s = \sqrt{12}\, f * \{N_{pe} * [(\theta_\pi - \theta_K)/n_\sigma]^2 - \Delta\theta^2_\pi - \Delta\theta^2_K\}^{0.5}$$

Assuming digital registration of the photon hits, Fig. 12 shows the pixel size corresponding to 2σ discrimination between π and K rings for the PMT detector as a function of particle momentum. For comparison, the pixel size needed by a pad readout wire chamber using TEA is also given in Fig. 12 by the dashed curve. The value used for N_{pe} is not the mean number of detected photons but rather the minimum number which can be expected with 90% confidence for each detector. The chromatic dispersion term, $\Delta\theta_{Chromatic}$, depends on photodetector bandwidth. It is taken to be either 23 μrad or 64 μrad for Ne radiator gas used with TEA or PMT detectors, respectively[37]. With a pixel size of 7.5 mm, 2σ π/K discrimination up to about 250 GeV/c is expected with the PMT. A wire chamber with pad readout using TEA would need a pad size of about 2 mm for similar performance.

To first order the size of the PMT array is given by the product of mirror focal length and the spread in track polar angles. In this approximation the size of each photomultiplier array is 90 cm in the horizontal and 180 cm in the vertical. Each array is covered by 240 PMT's similar to the R2489. With a pixel size of 7.5 cm, each multi-anode PMT would have 64 pixels. Thus the total channel count for the RICH is 480 PMT's with 31K pixels. We will assume one readout channel per pixel for the purposes of a cost estimate, although other techniques, such as delay line interpolation, charge division, etc., will be investigated as a means of reducing the number of readout channels.

In the SFT detector the deployment of a PMT array along a RICH mirror focal surface may be complicated by other considerations, such as background to other detector components generated in the material of the PMT array, or backgrounds to the detection of the Cerenkov photons caused by false signals generated by photons or charged particles passing through the tube array. In general, these are much more tractable in a fixed target configuration than in a collider experiment, especially since we plan to "hide" the tube array behind the steel of the analysis magnets. In spite of the relative ease of avoiding these problems, we plan to investigate light collection methods where the imaged photons are conducted over several meters of optical fiber bundles to a remotely located PMT array.

Finally, the manufacturability and long term stability of large mirrors produced on low mass substrates such as polycarbonate will be studied before committing to a mirror construction technique. We hope to minimize mirror mass which, through secondary interactions, is a minor source of background high p_t particles for other detector components. In any case there seems to be no problem with generating the necessary quality mirrors for the RICH by more conventional techniques, such the usual glass substrate.

In summary, it seems that Cerenkov photon detection employing an array of multi-anode photomultiplier tubes can provide performance comparable to that of the conventional gas filled wire chamber photodetectors. Furthermore, this performance can be obtained without the environmental difficulties associated with TMAE or the VUV losses associated with TEA. For this reason and for the speed of response the PMT is, at the moment, the preferred technique for the SFT RICH photodetector.

III.E Electromagnetic Calorimeter

The large phase space available to the decay of B hadrons favors high-multiplicity final states resulting in a high probability of one or more photons in the final state. The average photon multiplicity in a B decay is approximately five, with few exclusive channels not having photon decay products. Furthermore, the daughter D^{*0}, D^{*+}, and D^{*}_{s} decay almost entirely into electromagnetic final states. Hence, while B's that decay into electromagnetic final states are difficult to reconstruct because of the combinatorial problems of assigning the photons to a secondary vertex, they cannot be ignored. Even for $B \rightarrow J/\Psi + X$ decays, which have a particularly favorable ratio of all charged to mixed charge and electromagnetic decay products (roughly 50%), at least half of all decays contain a π^0. For generic types of B decay the ratio is much greater. Hence the ability to reconstruct electromagnetic final states can vastly increase the number of reconstructable B events. In

addition, good electron identification is needed for various aspects of B physics. Therefore, good electromagnetic calorimetry is important. (However, it is not as important to have hadron calorimetry since the SFT spectrometer is predicated on reconstructing every charged track in so far as that is possible.)

The criteria for the calorimeter are demanding, particularly for the forward elements near the proton beam. The SFT calorimeter must, first and foremost, be fast, since we plan to operate at rates exceeding 10^7 interactions per second. It must also have good energy resolution and position resolution. It should also have good resolving power for closely spaced photons for identification of π^o's. And the EM detector must survive for years subjected to high levels of radiation (Fig. 13). Although these criteria severely limit suitable technologies, there are several promising avenues of approach to the design of the electromagnetic detector. These include lead-fluoride, silicon, and scintillating fiber calorimetry (SCIFI). At this time we are not committed to any particular technology, but for purposes of this Expression of Interest, we detail the scintillating fiber option. Besides the qualities outlined above, SCIFI calorimetry has two other favorable features: it facilitates simple transverse segmentation, and it is inexpensive. It does not lend itself easily to longitudinal segmentation; hence we are considering the addition of a preradiator.

The EM detector is situated about 40 m from the target. As shown in Fig. 13, the calorimeter approximates a circular acceptance with octagonal geometry. It is 5.4 m in width and height and covers an area of 24.9 m^2. It is divided into three sections: inner, middle, and outer calorimeters, each having different lateral granularity in order to achieve uniform segmentation in rapidity. The entire array is composed of two sizes of lead/scintillating fiber modules: a 5.00 x 5.00 cm^2 size for the inner calorimeter, and a 10.0 x 10.0 cm^2 size for the middle and outer calorimeters. The total number of modules is 2,752. Each module is subdivided into multiple cells, the modules in inner and middle calorimeters being composed of 16 cells, and the modules in the outer calorimeter of 4 cells. The cells are square in cross section and have sizes: 1.25 x 1.25 cm^2, 2.50 x 2.50 cm^2, and 5.00 x 5.00 cm^2. Table III.A gives the channel count for each section. Although we have chosen a design which incorporates SCIFI calorimetry throughout the entire array, it is clear that the performance requirements are less severe as the radial distance from the beam increases. Hence a calorimeter using two different technologies, one appropriate for the inner high rate environment requiring high granularity, and the other for the much less severeouter calorimeter environment requiring less granularity, is under consideration.

Table III.A
SFT Electromagnetic Calorimeter Elements

Section	Area (m^2)	Cell Size (cm^2)	Channels	Phototubes	Modules
Inner	0.86	1.25 x 1.25	5,504	344	344
Middle	4.04	2.50 x 2.50	6,464	404	404
Outer	20.04	5.00 x 5.00	8,016	8,016	2,004
Total:	24.94		19,984	8,764	2,752

Table III.B gives the parameters of the lead/fiber matrix for the smaller SCIFI module. The larger module differs only in size. Lead has been chosen as the radiator material because it is cheap, easy to machine, allows a module with a short radiation length (0.91 cm) and Molière radius and a relatively long interaction length. We are considering using a less dense material for the outer calorimeter where the lateral shower size and the cell size are poorly matched. Each module is a square matrix of 1 mm diameter fibers embedded in lead. The fraction of fiber to lead (packing fraction) is approximately half (0.52). Each module is 30 radiation lengths and 1.11 interaction lengths in length. The packing fraction of 0.52 would give an energy resolution of about $\sigma(E)/E = 9\%/\sqrt{E}$. We expect a 2% constant term added to this. A larger packing fraction would give a better energy resolution, but would increase the Molière radius. For a central impact on an inner calorimeter cell, about 65% of the total energy would be contained within that cell.

Table III.B
SCIFI Small Module Parameters

Size:	5.00 x 5.00 x 27.3 cm^3
Packing fraction (by volume):	0.07 glue : 0.32 fiber : 0.61 Pb
Mass:	4,951 g
Radiation length:	0.91 cm (30.0 total)
Interaction length:	24.6 cm (1.11 total)
Channel diameter:	1.10 mm
Distance between fiber centers:	1.56 mm
Fiber diameter:	1.0 mm
Total number of fibers:	1,024 (32 x 32)
Total fiber length:	27,955 cm

Several different techniques of construction of the modules are being explored. Casting appears to be impossible to accomplish in a reliable manner. The alternative is to fabricate the modules by rolling PbCaSn (0.065% Ca and 0.5% Sn) alloy sheets and either gluing or soldering them together. This method has been used successfully in the construction of large scintillating fiber calorimeters[38,39]. Several firms that have experience in rolling lead sheets have made prototypes for us[40]. The mass of the entire calorimeter is estimated to be approximately 50,000 kg.

A schematic of what an inner calorimeter module might look like is shown in Fig. 14 The module has a clear plastic light mixer at the far end with an embedded fiber to be used for calibration purposes. It is followed by the lead-fiber matrix, which has the light readout system on the opposite end. The module is laterally subdivided into 16 cells. Each cell is 1.25 x 1.25 cm^2, providing excellent transverse segmentation. The light is brought to a multi-anode photomultiplier by a light guide which serves to mix the light.

The choice of fiber depends on the section of the calorimeter. For the inner calorimeter it is dictated by the requirement that it survive 10 Mrad of electromagnetic

radiation deposited in a year. At the present time research on radiation-hard scintillating fibers is proceeding at a furious pace. The current leader in radiation hardness is 3HF which appears to survive a dose of 10 Mrad[41]. There are several manufacturers who can produce 3HF scintillating fibers in large quantities[42]. Excellent quality scintillating fiber has also been manufactured at Fermilab for experiment E687 at a very modest price ($0.20/m)[43]. We anticipate the availability of more radiation-hard fibers before the construction of the SFT EM detector would start, but this is not required.

Crucial to this design is the performance of multi-anode photomultipliers. Although such devices have been on the market for several years, they have not yet seen widespread use in the high energy physics community. No current multi-anode photomultiplier has the pixel size we wish, but discussions with representatives from Hamamatsu indicate that existing multi-anode photomultipliers can be modified at a very moderate cost. The design of an entirely new device would cost on the order of $125K, not an unreasonable amount. We intend to procure and test several of the Hamamatsu R4089 multi-anode photomultipliers, which are very similar to what would be needed for the calorimeter described here.

The approximate cost of each of the three types of SCIFI modules would be: $2450, $2660, and $1260 respectively for the inner, middle and outer calorimeters. The prices for most of the components are based on prototyping by the E771 collaboration. This cost is dominated by the price of the photomultiplier and hence dramatically falls off as the cell size increases, with a price per cm^2 X_0 of: $3.30, $0.90, and $0.40 for the three different modules. The total cost of the calorimeter has been estimated using these figures and a cost of $30 per channel for additional electronics and $40 per module for calibration monitoring. The grand total is $5156 K for the entire EM detector. This is a modest amount for the size and performance of the detector.

Although there has been a recent explosion of interest in scintillating fiber calorimetry, almost all of the research has involved hadronic calorimeters. Such calorimeters have relatively poor electromagnetic energy resolution because of the small packing fraction (0.25) needed for hadron shower compensation. For the design of the SFT EM detector, we have increased the fraction of fiber to lead relative to that of hadronic calorimeters to obtain better electromagnetic energy resolution. However, because of the large photon energies at the SFT we expect to have to deal with effects which heretofore have been masked by the relatively poor resolution of the present SCIFI calorimeters. Such systematic effects will show up in the constant term of the equation for the energy resolution. At the present time, the SCIFI calorimeter designed for the JETSET collaboration has the best potential energy resolution. However, it has been tested (and will operate) at such low energies that the statistical error on the energy resolution dominates. An important objective for us is to construct and operate SCIFI prototypes at energies more nearly those which we must deal with in the SFT, addressing some of the technological issues pertinent to the use of scintillating fibers for calorimetry: lateral nonuniformity, fiber inhomogeneity, linearity, rate effects, and hadron contamination. We plan to do this in a real experimental configuration at Fermilab, where the radiation levels and interaction rates will be remarkably like those expected at the SFT, as well as in more controlled

situations.

Many of the issues concerned with reconstructing B events which decay into final states involving photons have not yet been properly addressed. Although much study has been done in this regard for B physics at e^+e^- colliders, little has been done concerning the hadronic production of B's. While the gamma multiplicities are daunting, the potential gain is enormous. For example, the CLEO II collaboration anticipates an increase of 10 to 20 in the number of reconstructed B mesons solely from their improved electromagnetic calorimeter[44]. The salient question we need to answer is exactly how much gain can one obtain from measuring electromagnetic final states in a fixed target environment. Some decay modes will clearly be easier than others. An example of this is given in Fig. 15 which shows plots of the energy of photons vs. their distance from the proton beam at the face of the calorimeter, for minimum bias events and photons from events with a $B \rightarrow K^*\gamma$. The gammas from the B decay clearly stand out. We intend to undertake a systematic study of what decay modes involving photons can be reconstructed given a model calorimeter such as the one briefly outlined above, and use the results to further refine the design of the calorimeter. We stress here that while the physics goals outlined in this Expression of Interest can be achieved without having electromagnetic calorimetry, its potential for increasing the number of B's deserves serious consideration.

III.F Muon Detector

As shown in Fig. 4, the SFT muon detector begins at 47 meters and extends to 68 meters from the target. The steel shield is divided into three sections with the muon energy loss of each of the three section approximately 10 GeV, 5 Gev and 4 GeV.(from upstream to downstream). The cross section of the downstream shield is smaller in tranverse size than the upstream ones such that larger angle tracks penetrate a steel thickness of approximately 15 GeV compared to 19 GeV for smaller angle forward muons. The other feature of the muon detector is the beam dump in which the 20 TeV proton beam is disposed. This dump is embedded in the muon steel and is made up of tungsten or uranium, as availability dictates. The general configuration of the dump is indicated by the black shaded area in the Fig. 4.

Embedded in the steel are three planes of resistive plate counters (RPC's)[45,46]. The RPC planes have dimensions 6.5m x 6.5m (42.25 m^2), 7.5m x 7.5m (56.25 m^2) and 8.0m x 8.0m (64.0 m^2) respectively. They operate in the streamer regime and are characterized by large electric fields between parallel plates of high volume resistivity (10^{11} ohms cm) and small (2 mm) gaps. A section of a plane is shown in Fig.16a. When ionization occurs, because of the large fields, a streamer is created in a very short time (rise times of a few ns) leading to excellent time resolution (<0.5 ns). Because of the high resistivity the discharge is limited to a small area (10 mm^2), providing rate characteristics that make them adequate even in the hottest area of the SFT muon chamber at rates greater than 10^7 interactions per second. The recovery time of the small area of the detector which experiences the streamer is of order 10 ms. The rate dependence of these devices ,which has been measured in tests done at CERN by the Pavia and Lecce groups[47], is shown in Fig. 16b. The actual signal shape is shown in Fig. 16c. Devices similar to the ones that we plan to use in the SFT muon detector have 95% efficiencies at 50 Hz/cm^2, the highest rate expected

anywhere in the SFT muon detector at 10^7 interactions per second.

The output of the RPC's comes from a pickup pad structure built into each module This pad structure is projective in both x and y dimensions. To recover slight geometric inefficiencies due to dead regions at the edges of the pads, each plane is constructed of two layers slightly shifted with respect to each other. The signals from the corresponding pads in each layer are discriminated and then ORed to produce the final pad signal. These chambers provide the input to the muon triggers as described in section III.G. The basic definition of a muon for the SFT is a triple coincidence of selected pads between the three layers of the RPC's.

The exact configuration of the pads is a matter for further study as the trigger algorithms are better defined, but a rough estimate of the number of pads per plane is approximately 8K (times 2 to take into account two layers/plane). The total number of pads is 48K. The electronic grouping of the pads for the trigger is set by the multiple scattering in the shield.

III.G SFT Trigger Strategies

Even with the considerable increase in the beauty cross section between present Fermilab fixed target energies and the 20 TeV SFT, the requirement for powerful triggers is still important both to restrict the amount of data logged and to minimize the number of events handled by the offline computing process. Fortunately, fixed target B production has enough striking attributes to enable the construction of very selective triggers. The relative ease of implementing triggers is a essential difference between doing B physics in a collider environment and doing B physics in a fixed target configuration.

The more prominent features of the B events that can be exploited for trigger purposes are:

1. The presence of a high p_t lepton (from the semileptonic B decays).

2. The presence of a high mass lepton pair (from the $B \rightarrow J/\Psi$ decays or the double semileptonic decays of the B and the $\overline{B}$).

3. The large total transverse energy and individual track transverse p_t.

4. The presence of secondary vertices.

It should be noted that all of the above conditions can be applied independently and, therefore, lend themselves to the natural implementation of a multilevel trigger.

Triggering on the characteristic features of B events can be accomplished using several different technologies in the various levels of the trigger process. Various trigger schemes are under consideration. For purposes of definiteness, we outline below a particular scheme which is based primarily on muon triggers at the first level, followed by

track reconstruction at the second level. Other trigger schemes will be examined but we give this as an example of the trigger effectiveness that can be achieved. The performance of the scheme is such that more than one out of every five to twenty events written to tape will be a B event.

III.G.1 SFT Muon Trigger Scheme

For some time muon triggers have been understood[4,5,48] to be a powerful means of selecting $B\bar{B}$ events while rejecting ordinary hadronic interactions. The accumulation of large data samples of important B decay modes can be accomplished by triggering on muons from semimuonic B decays and from triggering on other more specific modes such as $B \rightarrow J/\Psi \rightarrow \mu\mu$. Triggering on semimuonic decays has the attractive feature that B's accumulated in this manner are "tagged" by the charge of the muon, thus giving some information about the particle or antiparticle nature of the B.

The $B \rightarrow J/\Psi \rightarrow \mu\mu$ events are relatively rare but very distinctive. Dimuons from $B \rightarrow J/\Psi \rightarrow \mu\mu$ decays are one of the most striking manifestations of beauty production in hadronic interactions and serve as the most powerful method to separate beauty events from the rest of the total cross section. The trigger strategy proposed here takes advantage of the special attributes of $B \rightarrow J/\Psi \rightarrow \mu\mu$ decays to produce a trigger with a large rejection of backgrounds, yielding an extremely favorable ratio of triggers to interactions.

In addition, the dimuons act as a starting point for the offline analysis, reducing the amount of reconstruction that must be performed on each recorded event and enabling excellent offline rejection of backgrounds since the observation of a J/Ψ from a secondary vertex unambiguously insures that an event contains a $B\bar{B}$ pair. We also emphasize here that $B \rightarrow J/\Psi$ decays are among the most interesting from the standpoint of searching for CP violation in B decay. There are several decay modes ($B \rightarrow J/\Psi K^0_S$, $B \rightarrow J/\Psi \pi^+\pi^-$, $B \rightarrow J/\Psi \Phi$ for example) for which the final state is CP conjugate, making them the most promising avenue to measuring CP violation. This is discussed in more detail in Section IV.

The $B \rightarrow \mu + x$ semimuonic decays offer different challenges and opportunities. Two features of the $B \rightarrow \mu + x$ semileptonic decays are very different from the $B \rightarrow J/\Psi$ modes and are very important. First, as pointed out above, the charge of the muon "tags" the decaying B so that some knowledge is gained about its particle or antiparticle nature. This is important for both mixing and CP studies. In addition and most importantly, the $B \rightarrow \mu + x$ decays are far more copious than the $B \rightarrow J/\Psi \rightarrow \mu\mu$ decays. In events containing a $B\bar{B}$ pair, semimuonic decay will produce a muon approximately 23% of the time and approximately 42% of these muons will have a $p_t > 1.5$ GeV/c. Muons with a p_t this large are quite unusual; semileptonic decays of pions, kaons and charm produced in 20 TeV/c interactions contain muons with this magnitude of p_t in less than interaction in 10^4. Therefore, high p_t muons provide a distinctive signal on which to trigger as discussed below in Section III.G.3 and 4.

III.G.2 Implementation of the SFT Trigger Scheme

The trigger scheme chosen here for the purpose of illustration, leads to a very

effective global event selection, and could be easily implemented with present day technologies and at a moderate cost. The scheme calls for the recognition of one or more muons at Level I, to be followed by fast track reconstruction at Level II, both in the conventional proportional chambers and in the silicon microstrip detector. Level II will require both the presence of high p_t muons and hadrons as well as the presence of secondary vertices. Further filtering of the events could be performed with an online microprocessor farm, if necessary. The scheme presented here, including both geometric acceptance and detector/trigger algorithm efficiency, has a rejection factor of 10^4 while keeping approximately 18% of the $B \rightarrow \mu$ and 33% of the $B \rightarrow J/\Psi \rightarrow \mu\mu$ signal.

III.G.2.a Level I Trigger

Level I will require the detection of one or more muons, as defined by the triple coincidence of an aligned set of pads in the projective pad geometry of three or more layers of Resistive Pad Chambers (RPC), embedded in the steel of the SFT muon detector (see Fig. 4). The minimum energy required of a muon to penetrate the SFT muon detector steel and produce a signal in the RPC's is 19 GeV in the central part of the acceptance and 15 GeV at wider angles. Studies of simulated $\sqrt{s}$=193 GeV events show that the probability for a minimum bias event containing a muon with more than 20 GeV from π or K decays in flight is of order 1->2%. A further reduction of the Level I trigger rate can be achieved by imposing a very rough minimum pt requirement on the muons detected by the RPC's. In a scheme in which the accepted muon coincidences are defined by means of Programmable Logic Gate Arrays (PAL's)[49], it is trivial to include only three-plane patterns consistent with a given p_t threshold. Although the p_t resolution achievable at this level is limited, it is adequate to provide the additional factor (two or three) required to fit the trigger rate comfortably within the Level II bandwidth. Alternatively, one can achieve the same goal by imposing a threshold on the total transverse electromagnetic energy of the event as determined by the SFT EM detector. Level I would be pipelined and would take less than a couple of hundred nanoseconds.

III.G.2.b Level II Trigger

We plan to develop a Level II trigger for the SFT which would perform complete online tracking in a couple of microseconds. As presently planned, this trigger level will increase the rejection of the total cross section by:

1. Imposing the requirement that the muon have 1.0 to 1.5 GeV of transverse momentum and that several tracks with intermediate p_t be present in the event, thereby increasing the probability that the selected events contain high mass B hadrons. This requirement is very powerful as can be seen from Fig. 17, showing the lab angle vs. momentum for muons from $B \rightarrow \mu + x$ and $B \rightarrow J/\Psi \rightarrow \mu\mu$ as well as from π, K and charm semimuonic decays. The contours of constant p_t=1.5 Gev/c show the clean separation of the signal from the background.

2. Examining the silicon microvertex detector for the presence of secondary vertices.

Given that the above two conditions can be applied independently of each other, it will be possible to optimize the signal to background ratio of the accepted events by tuning the parameters of the two requirements.

The overall rejection to be provided by the Level II trigger is about a factor of 50, an extremely modest requirement in view of the many different event features on which the trigger can operate. Given an expected input rate of the order of 5×10^4 events/s into Level II, one should think in terms of a processing time of about 2 microseconds, which would limit the dead-time to 10% even without the added complication of a pipelined system. We envisage reaching such a time performance while accomplishing a full track recognition by making use of associative memory pattern recognition.

An associative memory is a reversal of the traditional mode of operating a memory. A standard memory is interrogated by presenting an address at its input, the output consisting of the memory contents of the addressed location. The reversed mode of operation would consist of presenting the memory with a piece of data (a "pattern") and obtaining in response the address, if any, where the data is located. Such a device, referred to as a "content addressable" or "associative" memory would be used for pattern recognition by pre-loading it with all and only the patterns corresponding to events of interest (a very small subset of all the possible patterns); at trigger time, the patterns generated by the hits in the detector would be presented to the memory, which would then quickly recognize if the pattern under question is among the valid ones it contains. The development of such devices has started, in an ad hoc fashion, for current experimental efforts. We plan to continue and expand this development to meet the needs of the Level II.

In the basic design, each elementary unit ("bit") of an associative memory consists of a standard memory cell with a comparator and a latch associated to it. A multi-bit "word" will have attached to it a global latch, which is the logic AND of all the individual bit latches. When a piece of data (or pattern) is presented to the memory, a bit by bit comparison takes place, simultaneously for all the words contained in the memory, and the results of the elementary comparisons are stored in the bit latches. A complete match of the input pattern with any of the ones pre-stored in the memory will result in the setting of the "word latch", signaling in this way the recognition of the input being one of the valid patterns. For many trigger applications, the fact that any word latch is set would be all the information that is required, but it is very straightforward to provide also information on which was the matched pattern (its "address") by means of a standard priority encoder connecting all the word latches. For practical applications, it is convenient to organize each memory location into separate sections, each one containing the information relative to a specific element of the detector (e.g. a chamber plane). In such a way, at trigger time, rather than forming all the possible combinations of the hits from the detector elements of interest to the trigger algorithm, it is possible to present the memory in parallel with the hits from the individual elements. As a result, the total time required to submit the whole event to the memory, looking for a match of one of the pre-stored patterns with any of the ones one can form with the hits of the particular event, will be simply determined by the hit multiplicity of the detector element with the largest number of hits. It should then be clear that, when designing an associative memory chip for a specific application, one of the fundamental

parameters is the number of different "sections" into which each memory location should be divided, together obviously with the number of bits in each section.

The development of Level II will proceed in several steps. The first step in the process consists of completing the studies of the SFT trigger algorithms and defining the inputs from the SFT in terms of number of detectors, number of channels/detector and number of distinct useful patterns. The second step will be the actual design of the custom IC's that constitute that actual memory chips. In addition, one will need to develop the ancillary modules that are required to integrate the basic memory boards into a working system, comprising interfaces between associative memory arrays and encoding electronics on one side and host computer on the other, sequencers capable of feeding hit lists into and extracting results from the memory boards, etc. As mentioned above, the feasibility of developing a custom integrated circuit operating as an associative memory has already been proved. A 256 bit chip, organized into 8 "eight section" words with 8 bits per section, is currently being employed to perform on-line track reconstruction for the Fenice experiment[50] at the Frascati electron storage ring. A higher density IC, containing 64 words of 5x12 bits each, to be employed in heavy flavor fixed target experiments at CERN and Fermilab[51], is in an advanced state of design.

As mentioned earlier, the Level II trigger consists of two independent parts, the first acting on the information from the microvertex detector and looking for the presence of tracks with large impact parameter, the second processing the data from pad and muon chambers downstream of the last magnet and searching for tracks carrying transverse momentum above a given threshold. The microvertex trigger algorithm calls for the recognition of straight tracks, a track being defined as a set of 4 or 5 aligned hits from a corresponding set of planes in the microvertex detector. Participating in the trigger will be a set of planes from the downstream part of the silicon tracking section. Whether the final implementation of the trigger can be limited to reconstructing tracks in a single view, or if two or more parallel systems, reconstructing tracks in separate views will be necessary, needs more detailed study. A knowledge of the primary vertex position is essential and can easily be obtained from the active target, e.g by recording the pulse height of groups of channels. The vertex coordinates would then be added to those of the silicon hits, effectively removing the effect of beam spot size from the impact parameter evaluation. The hits from the 5 chosen silicon planes would then be fed to a bank of associative memories in the fashion described above. Upon loading of all the hits, the memory would provide a list of the found tracks in a time determined by the total number of hits in the busiest plane. Assuming a conservative clock rate of 30 MHz and multiplicities of the order of 30, this would correspond to response times of the order of one microsecond. A further step through a look-up memory would provide a value of the impact parameter for all the found tracks. Simulations[51] performed for B production at present day fixed target experiments indicate that such a system can provide rejection factors as high as a few thousand for signal retention of the order of 50%. Given that in the present proposal we only need a factor of 50 rejection from the combined action of the impact parameter and the p_t triggers, we feel extremely confident about the viability of the proposed scheme. Concerning the size of the required memory chip, the scheme calls for memory cells of 5 x 12 bits (5 detectors each one consisting of up to 4000 channels), a figure that has already been realized in an existing

design of an associative memory chip. We estimate a total number of patterns on the order of few hundred thousand, a manageable quantity both from the size and cost points of view.

The algorithm exploited for the implementation of the p_t trigger is chosen to accommodate the track geometry generated by the proposed two magnet configuration. In such a set-up, production angles are conserved after travel through the two magnets, while the displacement of the twice deflected track with respect to a parallel line originating from the interaction point is a direct indication of the track's momentum. Consequently, a determination of a track's slope and intercept performed downstream of the second magnet will provide an estimate of the track's transverse momentum, provided there is also information available on the position of the production vertex. A further piece of information required by the trigger is provided by the muon detector, so that the system can identify the muon track among the ones reconstructed in the pad chambers. In summary, we plan to present to a bank of Associative Memories the list of hits from three pad chambers, one plane of muon detector and the encoded vertex position, determined in the fashion described in the discussion of the vertex trigger. The Associative Memories would have been pre-loaded with the list of all the possible physical tracks carrying a minimum transverse momentum, so that presenting to them the list of hits would result in an output list of found tracks, the muon track carrying a special flag if it was recognized. As for the case of the vertex trigger, a further step of running the found tracks through a look-up memory would provide a list of the track's transverse momentum values. This information can than be used to impose different p_t threshold criteria to the muon and hadron tracks for the purpose of attaining the required levels of signal acceptance and background rejection. The p_t resolution required of the system can be used to determine the sizes of pads in the chambers participating in the trigger. For the purpose of the present document, we assume to impose on the muon track a p_t cut of 1.5 GeV/c, with a p_t resolution of about 10% in the region of the cut. Fig 18, showing sample trajectories of particles carrying 0.5, 1.0, 1.5 GeV of transverse momentum for different production angles, gives an idea of the spatial resolution required from the pads. We have estimated that the required performance can be achieved with a system of three pad chambers, each one containing about 8000 pads. The Associative Memory cell of 5 x 12 bits required by the vertex trigger is equally suitable for the p_t trigger system, provided the 8000 pads of a chamber are divided into two groups corresponding respectively to hits above or below the mid-plane. The five elements fed into the memory array are respectively the three pad chambers, the muon detector and the encoded position of the interaction vertex. The total number of patterns needed to represent all the physical tracks with p_t above the required threshold is estimated to be of the order of a few hundred thousand.

III.G.2.c Level III Trigger

Level III of the trigger system, a microprocessor based farm, could be constructed using present day technology from VME based ACP I or II microprocessor modules. We presume, however, that more advanced and more powerful microprocessor based farms will be available. The farm would be used to assemble the events and do the logistics of moving events to permanent storage. Extra rejection factors, if needed, could be done at this stage since different detector components can be correlated with one another and sharper cuts can

be made in some of the parameters of the event.

III.G.3 Acceptances/Efficiencies of SFT Trigger Sequence for Beauty

The yields of B decays depend on geometric acceptances and on the efficiencies of the various elements of the spectrometer. These cuts naturally produce some loss of signal along with a diminution of background. In Table IV below, the cumulative effect of all the acceptances, efficiencies and cuts on the muons from $B \rightarrow J/\Psi \rightarrow \mu\mu$ and $B \rightarrow \mu + x$ decays have been estimated using Monte Carlo estimates of the efficiencies of various detectors . The geometric acceptances in Table IV have been calculated using PYTHIA for $B \rightarrow J/\Psi \rightarrow \mu\mu$ modes and semileptonic $B \rightarrow \mu + x$ modes. The muons are required to be in the acceptance of the spectrometer (3 mrad $< \theta <$ 75 mrad) and to have sufficient energy to penetrate the muon steel. A total of 85% of the $B \rightarrow J/\Psi \rightarrow \mu\mu$ and 87% of the $B \rightarrow \mu + x$ semileptonic decays satisfy this basic requirement. The efficiency of the Level I trigger for detecting these muons depends critically on the efficiencies of the resistive plate counters (RPC's). For purposes of calculating the trigger efficiency, we have taken an overall RPC efficiency of 95% for the entire muon detector acceptance, so that the efficiencies for single and double muons are respectively $(0.95)^3$ and $(0.95)^6$

The primary function of the Level II trigger is to impose a threshold on the muon transverse momentum. More stringent cuts are applied to the single muon events, where the signal is more copious and the background more severe than the dimuon events. We envision a p_t threshold of approximately 1.5 GeV/c for single muons and 1.0 GeV/c for dimuons. This would give acceptances on the order of 42% and 95% respectively. Detector efficiencies as they impact on Level II are expected to be 80%. Finally, the physics requirement of more intermediate p_t hadrons in the event as well as the requirement of secondary vertices when applied by the Level II machinery will select 70% of both the remaining single and dimuon triggers. The combined trigger efficiencies for Level I and Level II are 18% and 33% respectively for $B \rightarrow \mu + x$ and $B \rightarrow J/\Psi \rightarrow \mu\mu$.

Table IV
$B \rightarrow J/\Psi \rightarrow \mu\mu$ and $B \rightarrow \mu + x$
Muon Acceptances and Efficiencies

	$B \rightarrow J/\Psi \rightarrow \mu\mu$	$B \rightarrow \mu + x$
Level I		
Geometric Acceptance for muon tracks (including steel attenuation)	0.85	0.87
Level I detector efficiencies	0.74	0.86
Level II		
Level II detector efficiencies	0.80	0.80
Multihadron and Secondary Vertex Requirements	0.70	0.70
Level II P_t cut efficiency for muons	0.95	0.42
Composite Acceptance/Eff. for single or dimuons triggers	0.33	0.16

III.G.4 Expected Performance of the SFT Trigger System

In this section we give the expected performance of the SFT trigger system for single and dimuons using the acceptances and efficiencies listed above. The vast majority of the raw muon trigger rate is due to the decays of charged pions and kaons. Only at the higher levels of the trigger can the presence of charm decays be seen in the data. Using a variety of Monte Carlo simulations containing π,K and charm semimuonic decays, using PYTHIA as the event generator, we have estimated the performance of each level of our triggering system. The trigger rate reduction factors per interaction are shown in Table V below:

As can be inferred from the Table IV above and Table V below, reaching very high levels of rejection of the total cross section with good efficiency for accepting B's is straightforward in the SFT. The situation is to be contrasted with the situation in collider interactions where triggering is quite difficult because of the low momentum of the secondaries. At the nominal p_t thresholds we should achieve rejections of 10^{-4} and 10^{-5} for single and dimuon triggers respectively. Thus at an interaction rate of 1.3×10^7/s we expect 130 dimuon and 1300 single muon triggers per second of beam entering Level III. These rates together with the event size of 20 Kbytes furnish the criteria for determining the size of the Level III microprocessor farm and for determining the data logging capability required for the SFT spectrometer. If it is deemed necessary, significant increases in the efficiencies of the collection of $B \rightarrow \mu$ and $B \rightarrow J/\Psi \rightarrow \mu\mu$, relative to those given in Table IV, can be achieved at the cost of writing more triggers on tape.

Table V
Expected Trigger
Suppression Factors
per Interaction

Trigger Level	DiMuon Trigger	Single Muon Trigger
I	$O(10^{-4})$	5×10^{-3}
II	10^{-1}	2×10^{-2}
I * II	$O(10^{-5})$	$O(10^{-4})$

III.H The SFT Data Acquisition System

A 15% dead time of the SFT DA at the nominal operating point of 1.3×10^7 interactions per second, appears to be well within the capabilities of present day CAMAC or FASTBUS data acquisition electronics (either existing or under design). A worst case of 100 microseconds per event for collection and assembly of data from the various crates is achievable with today's equipment so we take this as a upper limit on the DA speed that can

be achieved in a system consisting of many parallel data paths (similar to many systems already existing). Using 100 microseconds, we see that we can process 1500 events per second with a dead time of approximately 15%. This is the bandwidth required to handle the events that arrive at Level III.

Assuming the Level III microprocessor system can process events at the rate of one every 200 ms and that the Level III farm must process 1500 events per second (ignoring the dead time), approximately 60 microprocessors of the ACP II type will be required.

Anticipating no filtering in the SFT Level III microprocessor level, 130 dimuon triggers and 1300 single muon triggers would have to be archived (approximately 20 Mbytes/sec). Using present day 8 mm tape technology (Exabyte II tape units) operating at a nominal 500 Kbytes/sec, we would require sixty 8 mm tape units to record 1500 events per second. However, it is almost certain much faster data storage technologies will exist at the time the SSC begins to operate. In any case, the requirements of the SFT appear to be modest enough that a system could be configured with today's options and this is what has been costed in Section VI.

III.I SFT Offline Event Reconstruction

While the efficiency of offline reconstruction must be estimated on a mode by mode basis (see Section IV for a specific example), a few general remarks can be made about the process. The reconstruction of charged tracks in the spectrometer for the events satisfying the triggers will be quite efficient because of the number of planes, the granularity of chambers and the two dimensional pad structure which will greatly aid pattern recognition. In the same way, the multiplicity of planes in the silicon microvertex detector will make track finding quite efficient. We estimate that overall efficiencies of 98% per track are quite achievable for tracks within the acceptance of the spectrometer (approximately 70% of the B's have all the decay products within the spectrometer and 45% of all $B\bar{B}$ have all decay products of both B's in the acceptance). The most difficult region to handle is, of course the region near the beam. To facilitate this, we have designed the charged particle tracking of the spectrometer with the small angle region of the acceptance covered by small spacing wire chambers. We anticipate no problem reconstructing tracks in the upstream region of the detector because of the silicon microvertex detector. There will be some loss of tracks due to hit sharing in the downstream portion of the spectrometer but we minimize it with the use of the smallest gap chambers possible in the small angle regions between M1 and M2. As the design progresses, we expect to fine tune the details of the acceptance vs. dead region question.

The issues concerning photon reconstruction are more uncertain at this point. The SFT EM detector will capture most of the photons within the acceptance with good energy resolution. The major problem will be one of combinatorics since we cannot use the secondary vertex to separate the B photons from the directly produced photons. This problem is not nearly as severe as in the case of a collider event since the SFT will have on average only ten π^0's in the EM detector, but it is still troublesome. However, once again

the fixed target geometry gives us an advantage. Because of the high energy of the B hadrons (averaging 445 GeV/c) and the moderate Q value of a 5 GeV/c^2 object there is a certain amount of "pointing" that can be utilized in trying to identify the π^0's associated with a given B to minimize the combinations in the various mass spectra that are formed. In the course of the further studies, this issue will be evaluated quantitatively.

The final general remark that we make concerning event reconstruction is that the detection of secondary vertices is quite efficient in this detector because of the large number of planes and the special attribute of the SFT that the B tracks themselves almost always pass through a few planes before decaying. Therefore, unresolved vertices are not as severe a problem at the SFT as in other types of B experiments.

III.J Offline Computing Requirements of the SFT

Given the SFT capacity for logging on tape, we can estimate the requirements for offline computing, assuming an SFT data acquisition capability of approximately 1500 triggers per second. Based on this assumption, the expected accumulation of events on tape per year is approximately 10^{10} events. While we plan to develop other (and perhaps less restrictive) trigger strategies in the future, it is instructive to estimate the computing needs of the SFT based on the events that we plan to accumulate using the muon trigger schemes.

The muon signatures for B events give a focus to the offline analysis. Because of this considerably less computer time is needed per event than for experiments which must search globally for evidences of secondary vertices and do complete reconstruction to determine if a secondary vertex is due to a B decay. The muon based B analysis strategies allow structuring of the analysis programs to filter with successively more and more sophistication. The number of remaining events will decrease dramatically at each stage. For purposes of estimating the computing time required for the analysis, we have assumed a mixture of single and dimuon triggers weighted toward single muons by the expected ratio of the single and dimuon triggers.

We have considered separately the analysis schemes that we would pursue for single and dimuon triggers to estimate the computing requirements of the SFT. We will express the needs of the various steps for both trigger samples in units of VAX780 years. A computing year will be taken to be 10^7 seconds for purposes of these estimates (Computing duty factor of 1/3).

First, to extract the B->J/Ψ->$\mu\mu$ decays, we must process offline approximately 1->2x10^9 dimuon triggers/year. As discussed below in Section IV we expect 1/150 to 1/45 of the dimuon triggers to be due to B->J/Ψ->$\mu\mu$. Since the data is so rich, we expect that a relatively simple three stage analysis procedure will isolate the B's with very little background. The steps in the dimuon offline data analysis process are:

1. The first step will be a fast filter program to determine if the dimuon has a mass greater than 2.5 GeV/c^2. This filter will select events containing J/Ψ's or determine if

both muons have a p_t greater than 1.5 Gev/c (to select events in which both B's have decayed semileptonically). This filter program, by computing a relatively crude dimuon mass to reject low mass pairs that slip through the trigger, can reduce the data sample by a factor of three at a rate of 250 ms per event on a VAX780. As an upper limit, the total computer time required to perform this first step for a year of data taking would be approximately 50 VAX780 years, passing 3->6x10^8 events on to subsequent analysis steps. This process is very efficient in preserving J/Ψ's so we expect to still have approximately 1->3x10^7 B->J/Ψ's in the trigger sample.

2. The second step in the offline analysis of the dimuon will be a second pass, higher resolution, three dimensional reconstruction of the dimuons followed by the reconstruction of both muon tracks in the silicon microvertex detector. The muon reconstruction in the pad chambers is estimated to take approximately one VAX780 second per event. The reconstruction of the muon tracks in the silicon vertex detector and determination of whether they come from a secondary vertex may take as much as 5 VAX780 seconds per event. Taking 10 VAX seconds as an upper limit for the entire process, we estimate approximately 300 VAX780 years to accomplish this step and a reduction of the data sample to essentially the 1->3x10^7 B->J/Ψ events.

Thus the total time to reduce the data sample to an essentially pure B->J/Ψ->$\mu\mu$ will be approximately 350 VAX780 years. This rather modest computer need is well within the usage of various Fermilab fixed target experiment operating at this time.

The single muon analysis scheme is more complex and less certain than that outlined above for the dimuon triggers. These triggers are very rich in B's (because of the relatively large branching ratio for the semimuonic decays). Indeed we expect 1/20->1/5 of all single muon triggers surviving the trigger scheme to be due to B->μ. With this richness of our trigger sample, the offline program is essentially dealing with the final analysis stage and we must eventually process approximately 10^9 B events for physics content. After a relative simple first step where we examine the muons in the 10^{10} triggers to see if they come from a secondary vertex we will proceed to complete event reconstruction This initial step should be a filter program which undertakes the complete reconstruction of the muon in both the downstream spectrometer and the microvertex detector in the fastest possible way. Assuming we can achieve 0.5 seconds per event for this process, we will require 500 VAX780 years for this process but obtain with good efficiency (greater than 70%) an essentially pure sample of 10^9 B->μ events which must be fully reconstructed. Complete reconstruction of 10^9 events will be a large computing load. We estimate at least one VAX780 minute per event, leading to a computing need of 6000 VAX780 years.

IV. Ability of the SFT to Meet Physics Goals

While the SFT (both beam and spectrometer) described above can only be considered to be preliminary, the model that we have outlined can be evaluated as an existence proof to demonstrate that there are technologies and techniques that makes possible the study of rare B decays and the measurement of CP violation in the B system. In Sections IV.A and IV.B, we evaluate the richness of the two different trigger samples, (the expected signal to background) at each level of the trigger and offline analysis, and the yields of B->μ and B->J/Ψ->$\mu\mu$ inclusive modes using the SFT. In Section IV.C, we evaluate the yields of B's produced in a year and in Section IV.D we discuss the performance of the SFT spectrometer in accomplishing the goal of precision measurement of CP effects. We take a particular exclusive mode, B->J/ΨK^0_S as an example of only one of many B->J/Ψ modes that are expected to have detectable levels of CP violating asymmetries. We also comment on the potential of the "tagged" B->μ events for CP violation measurements. In all these discussions we start with the expectation that between 1/1900 and 1/7700 of all $\sqrt{s}$ = 193 GeV interactions in the SFT microvertex detector target section will contain B's (see Table I).

IV.A B->μ+x

Approximately 23% of all BB events will produce at least one muon via the semileptonic decay modes and that muon will have a high p_t a large fraction of the time (50% with p_t >1.5 GeV/c at $\sqrt{s}$= 193 GeV/c). This large branching ratio and the large production cross section for beauty at the SFT leads to a large ratio (between $1/3.2\times10^4$ to $1/8.2\times10^3$) of B->μ+x events produced per interaction as shown below in Table VI.

Furthermore, the distinctive p_t of the muons from this decay and the fact that the B events should have secondary vertices makes possible powerful triggers and a very significant increase in the enrichment factor for the events we write to tape. From Tables IV and V, we estimate that we will have one B->μ decay event for every 5 to 20 triggers written to tape as shown in Table VI.

Offline, according to Monte Carlo studies, the requirement of a 30 micron impact parameter for the muon in the SFT silicon microvertex detector improves the signal to background by a factor of approximately 10, producing a ratio between 2/1 and 1/2 for the events surviving the first step of the offline analysis while keeping the majority of the events (greater than 90%) Finally, finding additional charged tracks which are part of the secondary vertex will further help to eliminate single muon candidates which due to mismeasurements appear not to originate at the primary vertex. The detection of additional tracks from the secondary vertex reduces the backgrounds by another factor greater than ten leading to a signal to background in the resulting data sample between 5 and 20 to 1.

IV.B B->J/ Ψ->μμ Data Sample

Because of the cumulative branching ratios, the portion of the dimuon triggers due to actual B decays is relatively small. Given the 1.1% branching ratio for B->J/Ψ + anything and the 6.9% branching ratio for J/Ψ->μμ, only 1.5×10^{-3} of the BB events will be collected by the dimuon trigger strategy (taking into account that there are two B's in every event). Therefore, only one event out of between 1.3 to 5.1×10^{6} interactions will have a B->J/Ψ->μμ decay.

However, the backgrounds to the B->J/Ψ->μμ events can be reduced more easily in the trigger and the offline analysis than the backgrounds to B->μ+x events, since the constraint of requiring J/Ψ's at secondary vertices is very powerful. The requirement for the dimuon to be a J/Ψ, by itself, eliminates a large portion of the background decay dimuons. To estimate this we note that the J/Ψ production cross section in 20 TeV/c interactions for the mixed Be/Si target region of the SFT detector is estimated to be approximately 6 μb (extrapolating the lower energy J/Ψ production cross sections using the technique of L. Lyons[52] and using an A dependence of $A^{0.93}$). As noted above, the $B\bar{B}$ beauty hadron production cross section in 20 TeV/c interactions is estimated to be between approximately 30 to 120 μb for the Be/Si target section mixture assuming a linear A dependence of the beauty production cross sections and using the third order beauty hadroproduction cross section calculations of K. Ellis[3]. Using a branching ratio for B->J/Ψ of 1.1 %, we estimate that between 1/18 and 1/5 of the J/Ψ's produced at $\sqrt{s}$=193 GeV are due to a $B\bar{B}$ event in which one or the other of the B's decays via a J/Ψ decay mode. Therefore, the major objective of the online trigger and the offline analysis will be to select events containing J/Ψ->μμ decays.

The trigger strategy outlined above for dimuons will lead very quickly to significant enrichment of the signal to background ratio. From Tables IV and V we obtain the signal to background ratios given in Table VI. We find that between one in 40 to one in 150 dimuon triggers that we write on tape will be due to B->J/Ψ->μμ. The first step in the offline reconstruction, a crude high mass requirement imposed on the muon pair, will further reduce this ratio to a better value than the one expected from the ratio of B->J/Ψ vs. the direct J/Ψ production cross asections since we have already required some evidence of secondary vertices in the events in Level II (which will tend to suppress the direct J/Ψ production). Ignoring this suppression for the time being, we expect to be in the range of 1/12 to 1/3 signal to background (or better) after the first step of the offline analysis with preservation of almost all the signal. This ratio should become much greater than 10/1 after the second step in the offline analysis; the requirement that the muon pair come from a secondary vertex.

In Table VI below, we summarize the enrichment factors that we expect to achieve from the trigger strategies and the offline analysis steps just discussed.

Table VI
Beauty Enrichment Factors at Various Levels

Level	DiMuon Trigger (signal = B->J/Ψ ->$\mu\mu$)	Single Muon Trigger (signal = B->μ +x)
BB/interaction	$1/7.7\times10^{3}$->$1/1.9\times10^{3}$	$1/7.7\times10^{3}$->$1/1.9\times10^{3}$
Produced signal/interaction	$1/5.1\times10^{6}$->$1/1.3\times10^{6}$	$1/3.2\times10^{4}$->$1/8.2\times10^{3}$
Accepted signal/ Level I	$1/8.1\times10^{2}$->$1/2.0\times10^{2}$	$1/2.1\times10^{2}$->$1/5.3\times10^{1}$
Accepted signal/Level I* Level II	1/150->1/40*	1/20->1/5*
Offline Step I Sig./background	1/18->1/5	1/2->2/1
Offline Step II Sig./background	>>10/1	5/1->20/1

*This is the enrichment factor for events written to tape

IV.C B Yields in the SFT

Assuming that 10^{7} seconds of operation at 10^{7} interactions per second represents a standard year of operation for the SFT, we expect to obtain 10^{14} interactions and produce 1.3×10^{10} to 5.2×10^{10} $B\bar{B}$ events per year. Taking into account branching ratios, we would then expect to have somewhere between 2.0×10^{7} and 7.8×10^{7} B->J/Ψ->$\mu\mu$ and 3.1×10^{9} to 1.3×10^{10} B->μ+x decays take place.

Of the produced B's which decay into these two inclusive channels, between 6.6×10^{6} and 2.6×10^{7} B->J/Ψ->$\mu\mu$ and 5.6×10^{8} to 2.2×10^{9} B->μ+x survive the trigger system and are written onto tape. The large majority of these inclusive decays survive the first steps of the offline analysis so that we have essentially this level of data available for CP studies.

IV.D Ability of the SFT for CP Violation Measurements

Since the measurement of CP violation is the ultimate test of a B physics experiment or strategy, requiring the largest sample of reconstructed B's, we will evaluate the potential of the SFT for performing that task as a measure of the power of the fixed target option. As a measure of the ability of the fixed target technique to make measurements of CP violation, we take, as a single example, the decay B^{0}->J/Ψ K^{0}_{S}. As mentioned above, this mode is an example of the generic B->f decays where f is a CP eigenstate.($CP|\bar{f}\rangle = \pm|f\rangle$) In the case of this mode, if there is CP violation ($\lambda \neq 0$), the task will be to distinguish

between time distributions of the form

$$e^{-\tau}(1 \pm \lambda \sin \Delta m \tau / \gamma)$$

where the ± refers to whether the parent B was a B or $\overline{B}$ and where τ is measured in units of B lifetime, γ. Integrating this time distribution over one half period of an oscillation $\tau = \pi\gamma/\Delta m$, we get a difference in number of events observed for B and $\overline{B}$ decays, ΔN which is proportional to the integral of the differences of these time distributions

$$\Delta N = N - \overline{N} \approx 2\lambda \cdot \int_0^{\gamma\pi/\Delta m} \{e^{-\tau} \sin(\Delta m \tau/\gamma)\}\, d\tau$$

$$= 2\lambda \{1 + e^{-\pi\gamma/\Delta m}\} \cdot \{\Delta m/\gamma\}/\{1+(\Delta m/\gamma)^2\}$$

In the same way we can get the sum of N and $\overline{N}$ distributions

$$N_T = N + \overline{N} \approx 2 \cdot \int_0^{\gamma\pi/\Delta m} e^{-\tau}\, d\tau$$

$$= 2 \cdot (1 - e^{-\gamma\pi/\Delta m})$$

and the asymmetry (for one half oscillation) between B and $\overline{B}$ is defined as the ratio

$$A = \Delta N / N_T$$

$$= \lambda \{ (\Delta m/\gamma)/(1+(\Delta m/\gamma)^2)\} \cdot \{(1 + e^{-\gamma\pi/\Delta m})/(1 - e^{-\gamma\pi/\Delta m})\}$$

Using the value of $\Delta m/\gamma = 0.78$ obtained by the Argus collaboration[53] for B_d, we can write the expected asymmetry as

$$A \approx 0.5\, \lambda$$

for the first half period of the oscillation. For Bs decays into CP eigenstates (assuming that $\Delta m/\gamma$ for B_S is approximately 1/5 of $\Delta m/\gamma$ for B_S), we get

$$A \approx 0.6\, \lambda$$

In order to measure these asymmetries with a statistical significance of a given number of standard deviations, we must accumulate a large number of events in the given exclusive mode under study. It can easily be shown that $N_T \approx (\#\sigma/A)^2$, where $\#\sigma$ is the number of standard deviations of significance desired in the measurement of the asymmetry.

Therefore, $N_T = (3/A)^2 = (6/\lambda)^2$ B_d plus $\overline{B}_d$ exclusive decays into a CP eigenstate are required to measure a three sigma decay asymmetry between the particles and

antiparticles, if we restrict our measurements to the first half period of an oscillation. For maximal CP violation (λ=1, A=0.5), N_T=36 events. There is, of course, no need to restrict our measurements to the first oscillation since the time distribtuions are well measured in the SFT. For a more reasonable choice of λ=0.3, A=0.15, N_T= 400 events (200 B's and 200 $\bar{B}$'s) are required. The preceding analysis, of course ignores systematic effects. However, with the time spectra for the particle and antiparticle decays well measured (with resolution of better than 0.05 picosecond), we can eliminate many of the troublesome problems (for example, different rates of production of B and $\bar{B}$'s) that accompany a simple counting experiment to determine a CP asymmetry.

As was indicated above, we expect to produce between 1.3×10^{10} and 5.2×10^{10} $B\bar{B}$ events per year when the SFT is operating smoothly. Of these B's, we expect 6.7×10^{6} to 2.6×10^{7} B->J/Ψ-$\mu\mu$ exclusive decays to survive the trigger and the early stages of the offline analysis. Assuming a hadronization ratio of 2/2/1 for $B_u/B_d/B_s$, (and neglecting the small fraction of the b quarks that will hadronize into either B_c or $\bar{B}$ baryons) 2.7×10^{6} to 1.0×10^{7} of the B-J/Ψ decays will be due to B_d->J/Ψ followed by the decay of the J/Ψ ->$\mu\mu$.

Using a branching ratio for B_d -> J/Ψ K^0_S estimated by Dunietz and Rosner[2] of approximately 0.05% (or approximately 5% of the total B->J/Ψ inclusive mode rate) and a branching ratio for the K^0_S->$\pi^+\pi^-$ decay of 69%, we expect between 9.3×10^{4} to 3.7×10^{5} of these decays per year, divided approximately equally between B and $\bar{B}$ (modulo CP effects and possible slight differences in production rates of B and $\bar{B}$). After requiring that the K^0_S decay in the first 5 meters of the spectrometer and allowing for the additional acceptance (beyond that of the two muons) for the two pions from the K^0_S decay, 42% of the B->J/Ψ K^0_S decays survive. Estimating a single track reconstruction efficiency of 90%, we arrive at a final number of decays for the CP study of between 2.6×10^{4} and 1.0×10^{5} reconstructed B_d->J/Ψ K^0_S ->$\mu\mu\pi\pi$ decays. The efficiency of tagging the particle or antiparticle nature or the parent B must be evaluated for these events.

Approximately 65% of these events survive the requirement that all the decay products of the other B in the event be in the acceptance of the spectrometer (in order to be able to reconstruct, at least partially, the other B for tagging the particle or antiparticle nature of the B undergoing J/Ψ decay). In making this estimate we have used a reasonable mixture of decay modes for the "other" B. This yields 1.7×10^{4} to 6.7×10^{4} B_d->J/Ψ K^0_S->$\mu\mu\pi\pi$ events with the "other" B decay products in the the acceptance of the spectrometer. By examining the decays of the "other" B in the event, tagging strategies may be developed that allow an estimate of the probability that the B_d was a particle or an antiparticle at t=0. The least ambiguous tag is the one that utilizes the fact that the "other" B was charged. Here the special feature of the fixed target configuration, ie that the B's themselves pass through many planes on average helps a great deal in the tagging process since the charged or neutral nature of the B's can be determined by direct observation of B's. If, by direct observation, we detect a B_u, we can use this information as a check on assignment of positive or negative charge to the B_u. Because of the good resolution of the SFT and the multiple measurements of every track, we expect to maintain a relatively low level of misidentifications of other tracks in the event and having the extra information about the

sum of the charges makes the probability of missing tracks or adding tracks negligible. To be in error we must incorrectly add or miss two tracks. Mistagging should be small under these conditions. We expect to achieve a good tag using B_u decays in more than 50% of the B_uB_d events

Given a hadronization ratio of 2/2/1, we have a 40% probability of having a B_u produced in association with a B_d. From the discussion above, we expect to be able to determine the charge of the B_u correctly more than 50% of the time. This leads to a data sample of somewhere between $3.4x10^3$ and $1.4x10^4$ B_d->$J/\Psi K^0_s$ where the K^0_s->$\pi^+\pi^-$ and the J/Ψ->$\mu\mu$ and in which the B_d is correctly identified as having been a B or $\bar{B}$ at t=0 by the presence of a properly identified B_u. Therefore, the statistics of tagged B-> $J/\Psi K^0_s$ events is approximately one to two orders of magnitude greater than necessary for detection of a 15% CP asymmetry at the three σ level in this relatively rare exclusive mode alone. Our estimate of the level of statistics required for a CP asymmetry measurement in this one particular decay chain agrees with global estimates given elsewhere[6].

This particular exclusive decay mode is only one of several B->J/Ψ modes which are accessible using much the same triggering and tagging strategy. In addition, we have ignored the possibility of retrieving information from the $B^0_{d,s}B^0_d$ configuration. However, as a lower limit on the information about CP asymmetry that we can extract from the B->J/Ψ K^0s mode, this analysis will suffice. The analysis sequence outlined in the paragraphs above is summarized in Table VII below:

Table VII

B^0_d->J/Ψ K^0_s
—>$\pi^+\pi^-$
——>$\mu\mu$

Condition Imposed	Event Sample
$B\bar{B}$ produced	1.3 ->$5.2x10^{10}$
B->J/Ψ->$\mu\mu$ ($7.7x10^{-4}$)	2.0 ->$8.0x10^7$
Trigger Acceptance (.33)	0.66->$2.6x10^7$
Hadronization to B_d (40%)	0.26->$1.1x10^7$
B_d->J/Ψ K^0_s (5% of B_d->J/Ψ +x)	1.4 ->$5.6x10^5$
K^0_s->$\pi^+\pi^-$ (69%)	1.0 ->$4.0x10^5$
K^0_s Acceptance (42%)	0.42->$1.7x10^5$
B->J/Ψ K^0_s Track Reconstruction (90%/track)	0.28->$1.1x10^5$
"Other" B Decay track Acceptance (65%)	1.8 ->$7.2x10^4$
Hadronization to B_u (40%)	0.7 ->$2.8x10^4$
Determination of Charge of B_u (50%)	0.34->$1.4x10^4$

There is another, more global, consideration of particle/antiparticle tagging strategy

that is particularly interesting for CP violation measurements in view of the single muon trigger scheme outlined in Section III.G for the SFT. Since we expect in one year of operation of the SFT to produce between 3.1×10^9 to 1.3×10^{10} B->μ+x semileptonic decays on which we plan to trigger with high efficiency, we expect to obtain trigger samples of 250 million to 1 billion semimuonic B events on tape in which all decay products of both B's are in the acceptance of the detector. The other B in the event, of course, will undergo the full range of B decays, some of which are expected to exhibit CP asymmetries. Therefore, this approach to the detection of CP violations allows us to examine all B decays (with cumulative branching ratios for their decay chains greater than approximately 10^{-5}) with large enough statistics to achieve a statistically significant measurement of CP asymmetries. As stated above, in 40% of these events we expect the B decaying into the trigger μ to be charged and, therefore, to provide an unambiguous tag of t=0 particle-antiparticle nature of the "other" B. In these events since we can directly observe the charge of the B, we do not have to depend on the tag derived from determination of the charge of the muon which is ambiguous because of mixing or because of undetectable B->D->μ decays.

For the other 60% of the BB configurations in which the B decaying semimuonically is neutral, the muon charge must be used to determine the particle or antiparticle nature of the "other" B. This tag is ambiguous since the neutral B undergoing semimuonic decay could have undergone mixing or could have decayed B->D->μ. In both cases the muon would now have the wrong sign and would lead to an erroneously tag . These uncertainties lead to what is referred to as a dilution effect since it leads to the misassignment of B's either as particle or antiparticle and a corresponding washing out of the CP asymmetries. In the case of the B->D->μ decays, the number of false tags will depend on the ability of the microvertex detector to resolve secondary vertices. For the SFT, this resolution is thought to be very good because of the number of measurements which are possible, the low multiple scattering and the special attribute of the fixed target experiment where the B's and D's pass through many measurement planes before decaying. These factors make the probability of having an undetected B->D decay negligible.

The misidentification due to mixing effects is much harder to eliminate. To an extent these effects can be allowed for by assigning a B or $\overline{B}$ probability to each event (based on the decay length of the semileptonic decay of the neutral B). In this way the remaining 60% of the $B_{d,s}$->μ triggers can be used to complement the B_u->μ tagged sample.

Because of the enormous statistics of B->μ decays and large acceptance of the SFT for all decay products, these data samples represent an excellent opportunity to look for CP violation effects with high statistics in many or all B decay modes. These searches may prove even richer than the directed searches represented by our strategy of observation of B->J/Ψ decays in $B_u B_d$ events. Either strategy as well as many other trigger schemes will be feasible using the SFT spectrometer described above.

V. SFT Milestones/Key Events

The sequence of events that may lead to a Super Fixed Target B Facility has already begun. A significant step was taken recently with the inclusion of adequate land in the East Campus of the SSC to allow for the SFT. We have prepared a very schematic schedule for proceeding on the implementation of the Super Fixed Target Facility following the general guidelines of the SSC management. We would hope to accomplish the following goals by dates indicated below:

Development of first order ideas for the SFT	Feb, 88-May 1990
Inclusion of adequate land in East Campus footpad -	April,90
Submission of EOI	May 25, 90
R&D/Prototyping Phase begins for RICH/EM Cal/Triggers	June,90
Quantitative evaluation of the extraction system efficiency finished	August, 90
Conceptual Design/Extraction system finalized (Snowmass)	Sept,90
Particle Tracking Simulations of Crystal System finished	Nov., 1990
Testing of prototype RICH and Calorimetry elements (FNAL FT run)	Nov.,90->April,91
Testing of extraction system concepts (FNAL FT run)	Nov.,90->April,91
Associative memory chip available in quantity	April,91
Final choices for detector components	May, 91
Large prototype preparation for 1992 Fermilab FT run begins	May, 91
Conceptual design of the SFT spectrometer and components finished	October,91
Submission of SFT Proposal	Fall, 91
Prototypes of RICH,EM det,associative memory trigger and other SFT components ready for 1992 FNAL FT run)	Fall,92
Prototype crystal extraction system ready for testing in 92 FNAL FT run	Fall,92
Beam Transport Design finished	Spring,93
Experimental hall design finalized (including beam enclosures)	Spring,93
Design of final SFT spectrometer components begins	Spring,93
Design of final crystal extraction device begins	Spring,93
Design of Detector components complete/construction begins	Spring,94
Design of crystal channeling device finished/construction begins	Spring,94
Beam Transport Tunnels and Experimental Hall construction begins	Spring,96
Beam Transport Tunnels and Experimental Hall ready for occupancy	Spring,97
Final SFT Detector Components ready for beam testing at FNAL or the SSC	Spring,97
Installation of SFT beam transport	Fall,97
Installation of the SFT Spectrometer begins	Fall,97
First Circulating beam at the SSC	1998
Extraction System Testing begins	1998
Tuning of the SFT Spectrometer	1998
First run of SFT Spectrometer	1999

VI. Cost Estimates

While other potential technologies and techniques may be used to implement parts of the SFT, we have taken, as a model, the spectrometer and the trigger scenario outlined above for preparing a cost estimate for the various components of the SFT. These budgetary cost estimates are based, at the present time, on previous experiences rather than engineering studies and must be considered to very preliminary. Except for the SFT beam transport elements, no account has been taken of the possible availability of existing equipment appropriate for use in the SFT (such as magnets, electronics). We have mainly costed items based on 1990 technologies and have invoked economies due to expected evolution of technology or economies of scale in only one or two places. In spite of this, the entire cost of the SFT, including the costs of the beam transport and the experimental hall is many times less than the cost of even the most frugally designed 4π collider detector. All amounts are in 1990 dollars.

VI.A Extraction/Beam/Experimental Hall

1. Extraction System		
Dogleg SSC Dipoles	$ 300K	
Channeling crystal and assembly	$ 100K	
Lambertson System (including PS's)	$ 640K	
		$1040K
2. Beam Transport		
Transport Encl (3000m @ $2970/m)	$8900K	
Dipoles (6)*	-	
Quadrupoles (3)*	-	
Vacuum system	$ 50K	
Beam Instrumentation	$ 20K	
Total Beam Transport Costs		$8970K

*Presumed to be available from SSC culls and, therefore, not costed

3. Experimental Area		
Civil Construction (100mx20m x15m)	$ 4900K	
Crane (20 Ton)	$ 100K	
Electrical Installation (6 MW's)	$ 400K	
Counting room (40mx20m)	$ 420K	
Total Experimental area cost		$5820K
Total Cost of Extraction/Beam Line/Experimental Hall		$15830K

VI.B. SFT Spectrometer

1. Analysis Magnets*	
M1 analysis magnet	$1010K
M2 analysis magnet (including PS)	$2090K

M1 and M2 auxiliary systems		
(power supplies, refrig.,LCW water etc)	$ 300K	
Total Magnet Costs		$3400K

* We have costed the superconducting version of the magnet system although the conventional system if produced in the Dubna shops may be as much as a factor of five cheaper than the superconducting solution.

2. Silicon Microvertex Det. and Assoc. Elect.		
SMVD Target planes (30 @ $6K ea)	$ 180K	
SMVD Track planes (30 @12K ea)	$ 360K	
Mechanical mount/cooling/racks etc	$ 150K	
Associated electronics (2.4×10^5 chan)	$4800K	
Total Silicon Microvertex detector		$5490K
3. Tracking Sys and Assoc Elect.		
Beam PWC's b1,b2,b3,b4,b5,b6 (Mech.)	$ 150K	
Straw Tube Chamb. s1,2,3,4 (Mech)	$ 160K	
Pad Chamb. p1,p2, p3 (Mech)	$ 225K	
Straw Tube TDC's (84K @$20 ea)	$1680K	
PWC Amp/Latch System (54K @$20 ea)	$1080K	
Gas System	$ 50K	
High Voltage System	$ 90K	
Total Tracking System		$3165K
4. RICH Counter and Assoc. Elect.		
Prototyping Phase	$ 300K	
Mirrors: 80 cm x 80 cm @ $5K ea (56)	$ 280K	
Radiator Gas System	$ 50K	
Radiator Vessel	$ 180K	
Phototubes (480)	$1440K	
Readout Electronics (31K channels)	$ 780K	
Total SFT RICH Cost		$3030K
5. Electromagnetic Cal. and Assoc. Elect.		
Prototyping Phase	$ 400K	
Section 1: 344 modules @ $2448	$ 842K	
Section 2: 404 modules @ $2657	$1073K	
Section 3 2004 modules @ $1263	$2531K	
Electronics:19984 channels @ $30	$ 600K	
Calib. elec. 2752 @ $40	$ 110K	
Total SFT EM Detector		$5556K
6. SFT Muon Detector		
Shield Steel (1765 tons @150/ton)	$ 265K	

Resistive Plate Detector Planes (3)	$ 148K		
Electronics			
Discriminators (32K @$5 ea)	$ 160K		
Programmable Logic (8K config)	$ 160K		
Delays (32K @ $4 ea)	$ 128K		
Readout Architecture (crates/controllers)	$ 150K		
Cabling/Connectors	$ 190K		
HV System	$ 82K		
Gas System	$ 100K		
Transporters	$ 30K		
Total SFT Muon Detector Cost		$1413K	
7. Trigger and Filter Electronics			
Level I trigger	$150K		
Level II trigger:			
Associative Memory chip development and prototype	$ 80K		
Vertex trigger:			
300,000 memory cells	$ 90K		
crates + control logics	$ 75K		
P_t trigger:			
300,000 memory cells	$ 90K		
crates + control logics	$ 75K		
Cables, connectors, misc	$ 30K		
Total SFT Trigger Cost		$ 590K	
8. Data Acquisition System			
Local VAX cluster	$200K		
VME crates/Power Supplies	$ 60K		
Exabyte II Drives (60)	$164K		
Tape Controllers	$ 33K		
ACP II micro's (60)	$360K		
Buffer memory	$ 32K		
Total SFT DA Cost		$849K	
Total Cost of SFT Spectrometer			$23763K

VII. Summary

In summary, the SFT appears to be a very economic way of achieving a large production of $B\bar{B}$ events combined with good reconstruction efficiency. With this facility one can address all issues of B physics including rare decays and CP violation measurements in many modes with large statistics. The Lorentz boost of the produced B's gives unique advantages in the triggering, reconstruction and tagging of the B's. Finally, the limited solid angle coverage required by the SFT spectrometermakes it a very economical option compared to many other methods, most of which cannot approach the quality of the CP violation measurements possible in the SFT.

References

1. See, for example, B. Cox, F. Gilman and T. Gottschalk, Physics of the Superconducting Supercollider, Snowmass, 1986, eds. R. Donalson and J. Marx, 33(1986); J.D.Bjorken, Fermilab-Conf-88/134-T(1988) and many,many other sources.
2. See, for example, J. Rosner and I. Dunietz, Phy. Rev. **34**,1404(1987) or B. Cox, Fermilab-Conf-88/33(1986) or Annals of the New York Academy of Sciences, Vol. **535**, 224(1988).
3. K. Ellis, Workshop on a 20 TeV Fixed Target Reauty Facility at the SSC, (Nov.,1989).
4. B. Cox and D. Wagoner, Physics of the Superconducting Super Collider, Snowmass, 1986, eds R. Donaldson and J. Marx,83(1986).
5. Report of the Fixed Target Hadronic Spectrometer Working Group, Proceedings of the Conference on Physics at Fermilab in the 1990's, Breckenridge,Col., (Aug, 1989), to be published.
6. See, for example, K. Foley et al., Experiments, Detectors and Experimental Areas for the Super Collider, Berkeley, Cal., eds. R. Donaldson and M.G.D. Gilchriese, 701(July, 1987), A. Boden and A. Fridman, University of Cal Preprint UCLA-HEP-89-002.
7. B. Cox et al., Proceedings of the Summer Study on High Energy Physics in the 1990's, Snowmass, Col., eds. S. Jenson, 536(June,1988).
8. See, for example, "Relativistic Channeling", R. A. Carrigan and J. A. Ellison, eds. Plenum (1987).
9. E. Tsyganov, Fermilab TM-682, (1976).
10. See, for example, Elishev et al., Phys. Lett. **88B**, 387(1979); Gibson et al, Nucl. Inst. Meth. **B2**, 54(1982); Bak et al, Nucl. Phys. **B242**, 1(1984); Forster et al, 4 Nucl. Phys. **B318**, 301(1989).
11. S. I. Baker et. al., Nucl. Inst. Meth. **A248**, 301(1986).
12. V.V. Avdeichikov et al., Fermilab FN-429(1986); Translation of Dubna #1-84(1984); M.D. Bavizhev et al., Serpukov 89-77 (1989).
13. B.Newberger, Inst. for Fusion Studies Report, IFSR-429, (1990).
14. J. Ellison, Nucl. Phys. **B206**, 205(1982).
15. N. Kudo, Nucl. Inst. Meth. **189**, 609(1981).
16. B. Newberger, submitted EPAC 90.
17. B. Newberger, Inst. For Fusion Studies Report, IFSR-492 (1990).
18. SSC CDG, SSC-SR-2020, (1986).
19. A.M. Taratin, S.A. Vorobiev, M.D. Bavizhev, I.A. Yazynin, "Computer Simulation of a Many Turn Output of a Beam from an Accelerator with a Curved Crystal", Dubna Preprint.
20. N. Merminga and R. Ruth, Bull. Am. Phys. Soc. **35**, 984(1990).
21. T. Collins, FNAL TM-1407, (1986).
22. A. Chao et al., PRL 61, 2252(1989)
23. M. Harrison, Physics of Particle Accelerators, AIP Proceedings **184**, Vol 2, 2009(1989).
24. SSC CDG, SSC-SR-2020, (1986).
25. C. Wilburn, Micron Semiconductor, private communications.

26. S. Shapiro, Stanford Linear Accelerator Center, private communications.
27. M. Nakamura et al., Nucl. Instr. and Meth. **A270**, 42(1988).
28. D. Christian et al., IEEE Trans. on Nuclear Sci. **NS-36**, 507(1988); C. Swoboda et al., "A High Rate FASTBUS Silicon Strip Readout System, IEEE Trans. on Nuclear Sci., San Francisco, (Jan, 1990), to be published; R.J. Yarema and T. Zimmerman, A High Speed, High Gain Preamplifier System for Silicon Strip Detectors, IEEE Trans. on Nuclear Sci., San Francisco, (Jan, 1990), to be published; A High Speed, Low Noise ASIC Preamplifier for Silicon Strip Detectors, IEEE Trans. on Nuclear Sci., San Francisco, (Jan, 1990), to be published.
29. R. Chechik and A. Breskin, Nucl. Instr. and Meth. **A264**, 251 (1988).
30. S. Majewski, et al., Nucl. Instr. and Meth. **A264**, 235 (1988).
31. A. Breskin, Symposium on Particle ID at High Luminosity Hadron Colliders, FNAL, (April 1989).
32. R. Arnold, et al., Nucl. Instr. and Meth. **A252**, 188 (1986).
33. J. Seguinot, Symposium on Particle ID at High Luminosity Hadron Colliders, FNAL, April 1989.
34. M. Adams, et al., Nucl. Instr. and Meth., **A217**, 237 (1983).
35. T. Ekelof, 1984 SLAC Summer Institute, CERN-EP/84-168.
36. G. Coutrakon, et al., IEEE Trans. Nucl. Sci., Vol **33**, no. 1, 205 (1986).
37. T. Ypsilantis, Symposium on Particle ID at High Luminosity Hadron Colliders, FNAL, April 1989
38. D.W. Hertzog et al., Workshop on Scintillating Fiber Detector Development for the SSC, Fermilab, November 14-16, 385(1988).
39. D. Acosta et al., CERNB-EP/90-37(1990).
40. Action Tool+Die, Co., 3374 Precision Drive, Rockford, IL.
Vulcan Lead, 1400 Pierce St., Milwaukee WI.
41. C. Zorn et al., Nucl. Instr. and Meth. **A276**, 58(1989).
S Majewski et al., Nucl. Instr. and Meth. **A281**, 500(1989).
42. Bicron Corp., 12345 Kinsman Rd., Newbury, Ohio; Kyowa Gas, Chemical Industry Co., Tokyo, Japan.
43. A. Bross, private communication.
44. J. Mueller, private communication.
45. R. Santonico et al., Nucl. Instr. and Meth. **187**, 337(1981).
46. R. Santonico et al., Nucl. Instr. and Meth. **A263**, 20(1988).
47. M. Bertino et al, Nucl. Instr. and Meth., **A283**, 654(1989).
48. W. Selove, The Single Muon Trigger for E771, Penn Preprint UPR-161E.
49. W. Selove et al., Implementation of the E771 Level 1 Muon Trigger System using PLA Technology, unpublished.
50. M. Dell'Orso and L. Ristori, Nucl. Instr. and Meth. **A278** (1989) 436.
51. A. Lusiani, Pisa University Doctorate Thesis, 1988.
52. L. Lyons, Massive Lepton Pair Production in Hadronic Interactions and the Quark Model, Progress in Particle and Nuclear Physics 7, 169(1981).
53. Albrecht et al., Phys Lett **B192**, 245(1987).

Figures

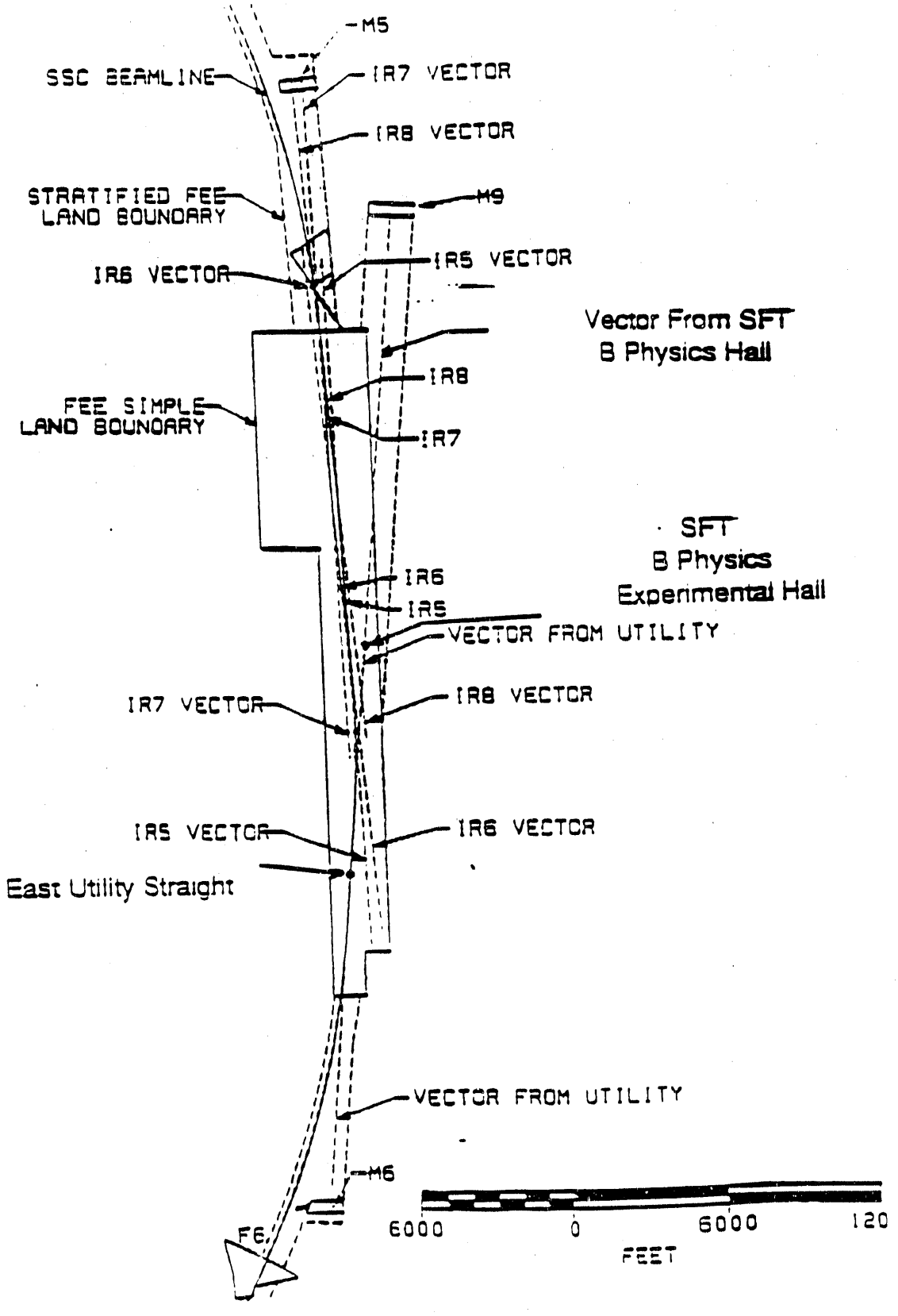

East Campus Siting of
20 TeV Super Fixed Target B Physics Facility (SFT)

Fig. 1

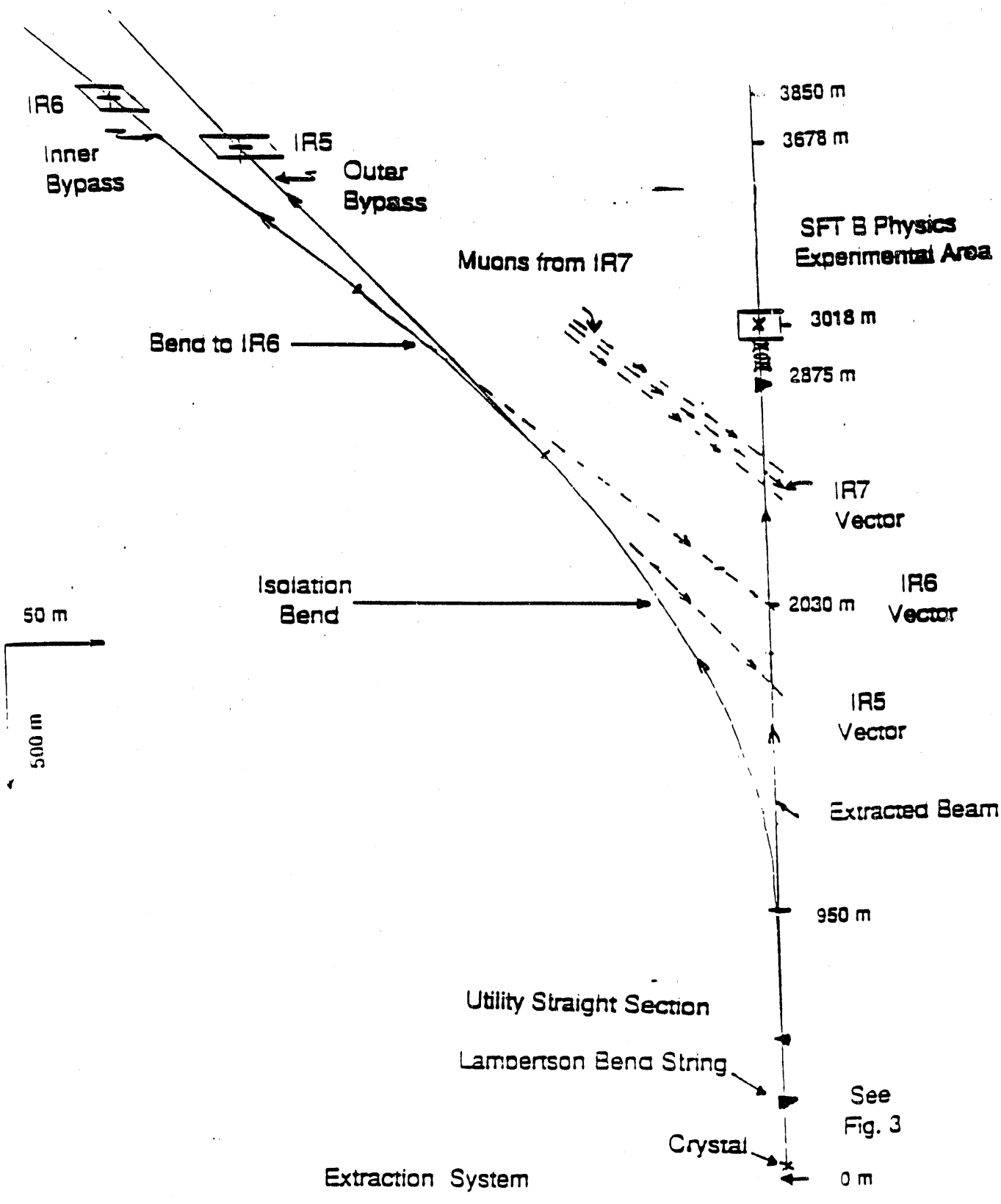
IR6
Inner Bypass
IR5
Outer Bypass
Muons from IR7
Bend to IR6
Isolation Bend
50 m
500 m
3850 m
3678 m
SFT B Physics Experimental Area
3018 m
2875 m
IR7 Vector
IR6 Vector
2030 m
IR5 Vector
Extracted Beam
950 m
Utility Straight Section
Lamberson Bend String
See Fig. 3
Crystal
0 m
Extraction System

Fig. 2

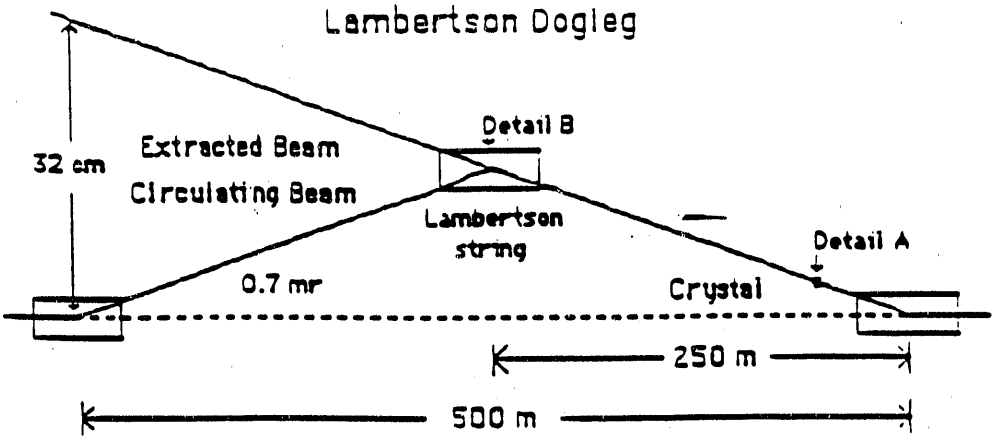

Detail A

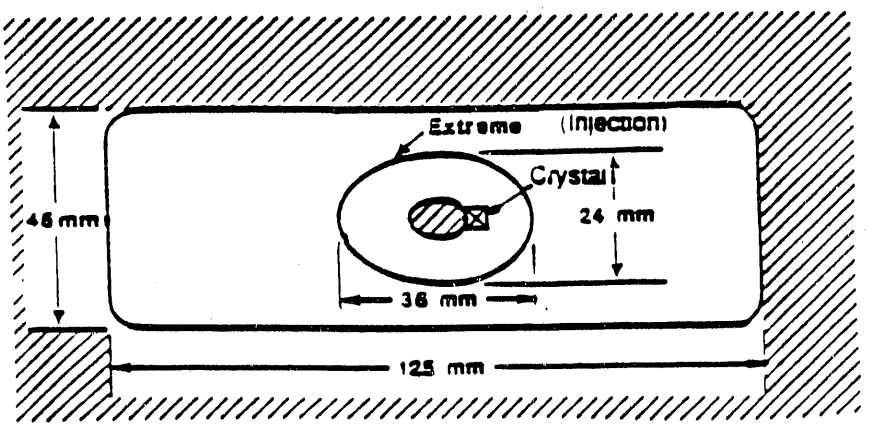

Detail B

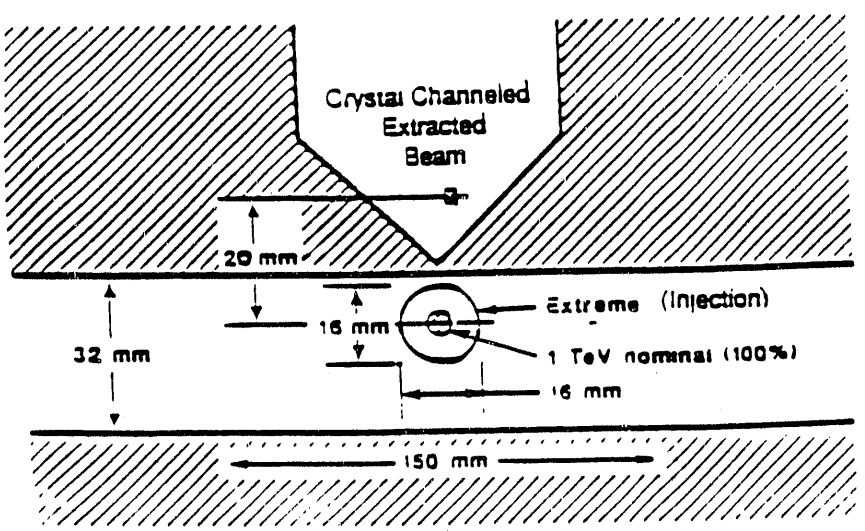

Fig. 3

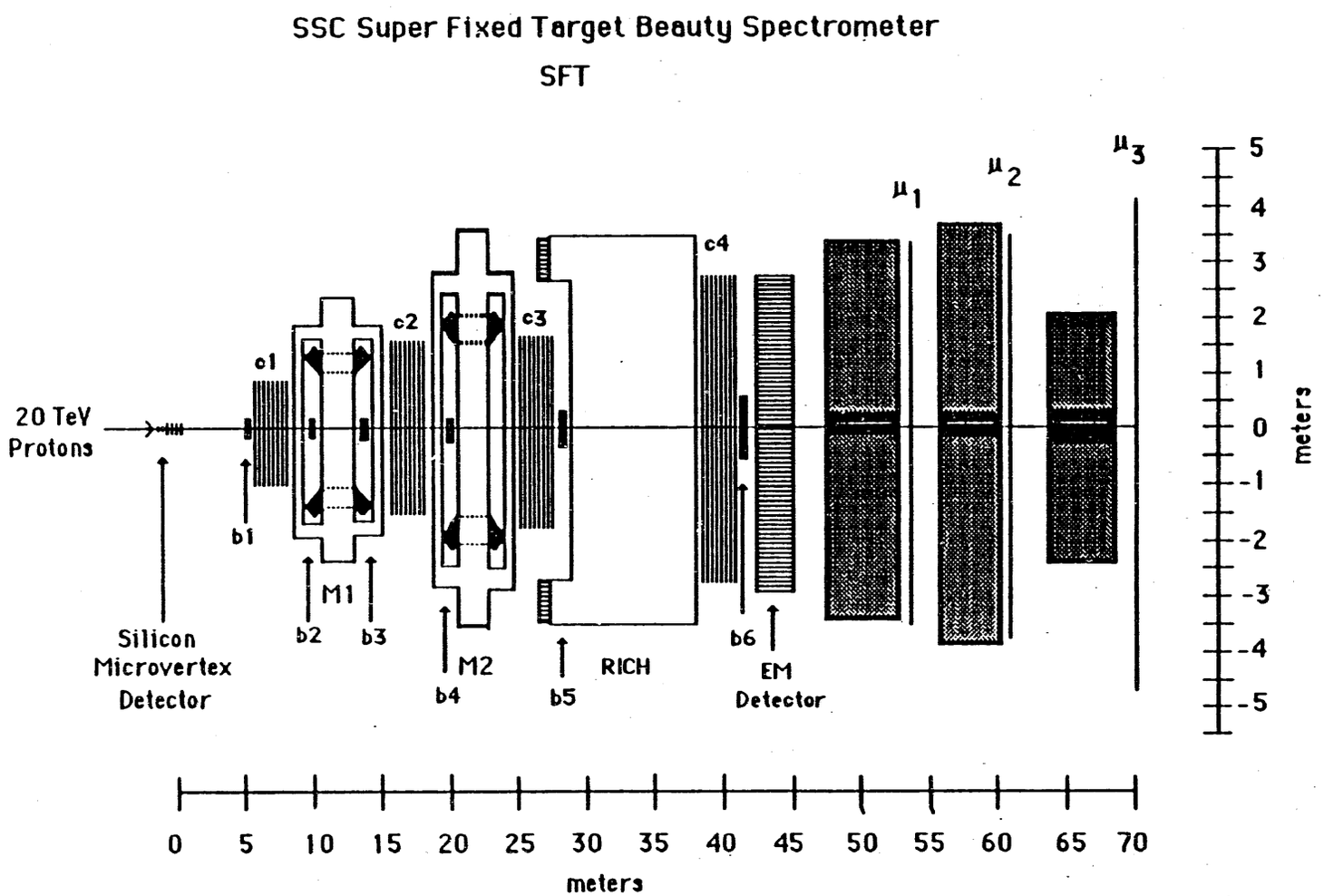
SSC Super Fixed Target Beauty Spectrometer
SFT
20 TeV
Protons
Silicon
Microvertex
Detector
b1
c1
M1
b2
b3
c2
M2
b4
c3
b5
RICH
c4
b6
EM
Detector
μ1
μ2
μ3
meters
0 5 10 15 20 25 30 35 40 45 50 55 60 65 70
meters

Fig. 4

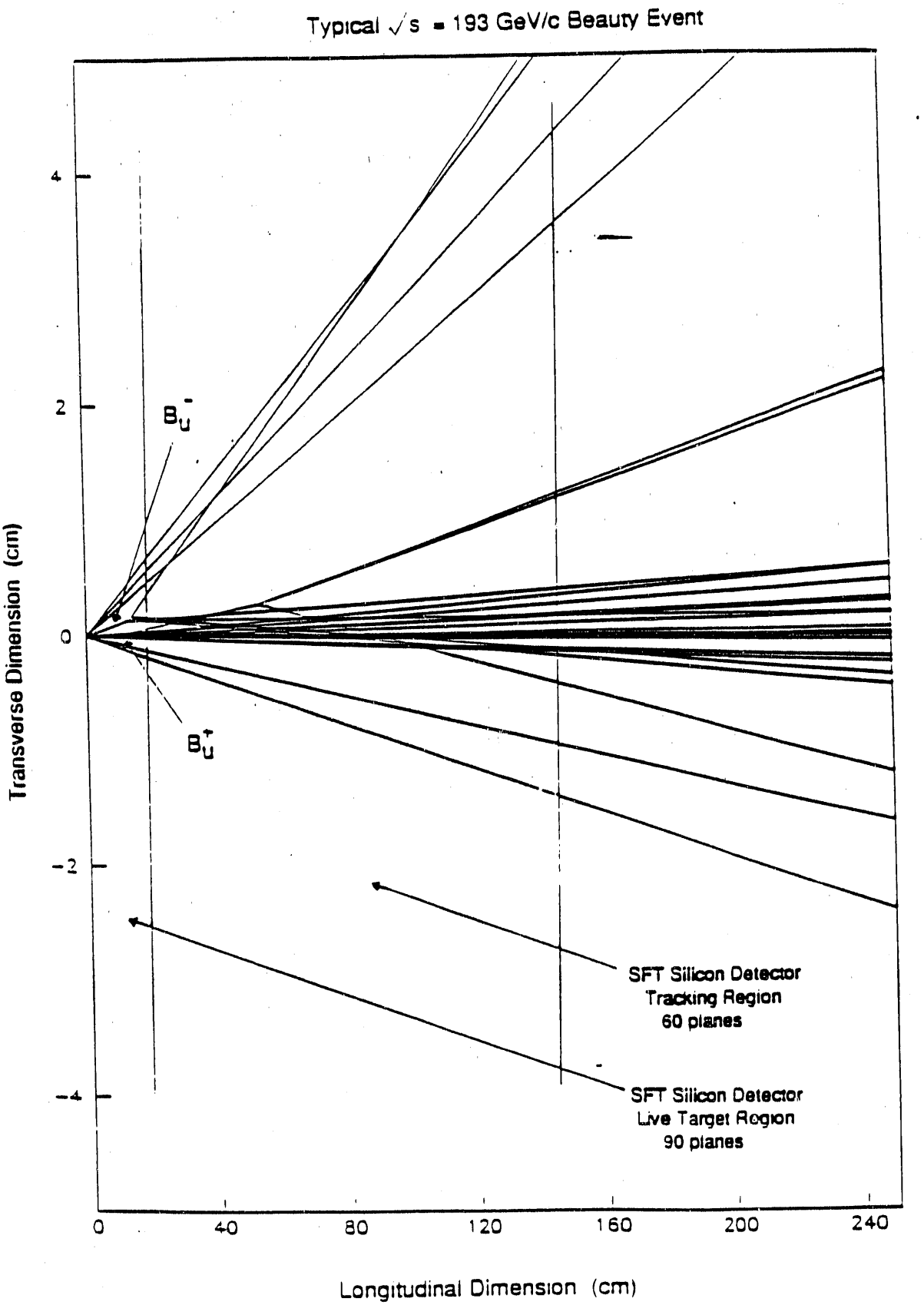
Typical √s = 193 GeV/c Beauty Event
Transverse Dimension (cm)
4
2
0
-2
-4
B_u^-
B_u^+
SFT Silicon Detector
Tracking Region
60 planes
SFT Silicon Detector
Live Target Region
90 planes
0
40
80
120
160
200
240
Longitudinal Dimension (cm)

Fig. 5

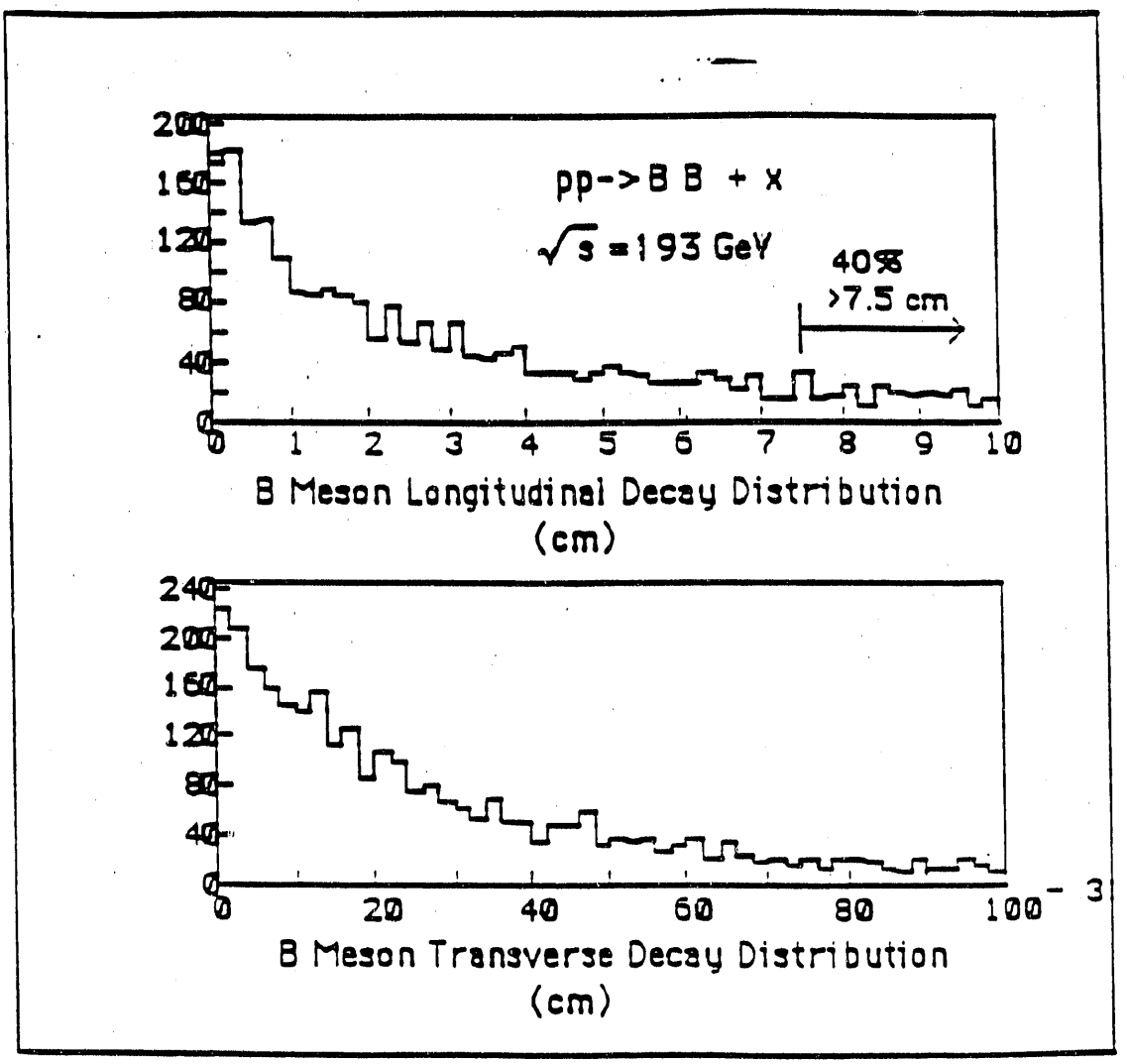
pp->B B + X
√s = 193 GeV
40%
>7.5 cm
0
40
80
120
160
200
0 1 2 3 4 5 6 7 8 9 10
B Meson Longitudinal Decay Distribution
(cm)
240
200
160
120
80
40
0
0 20 40 60 80 100
B Meson Transverse Decay Distribution
(cm)

Fig. 6

Bending Dechanneling Losses

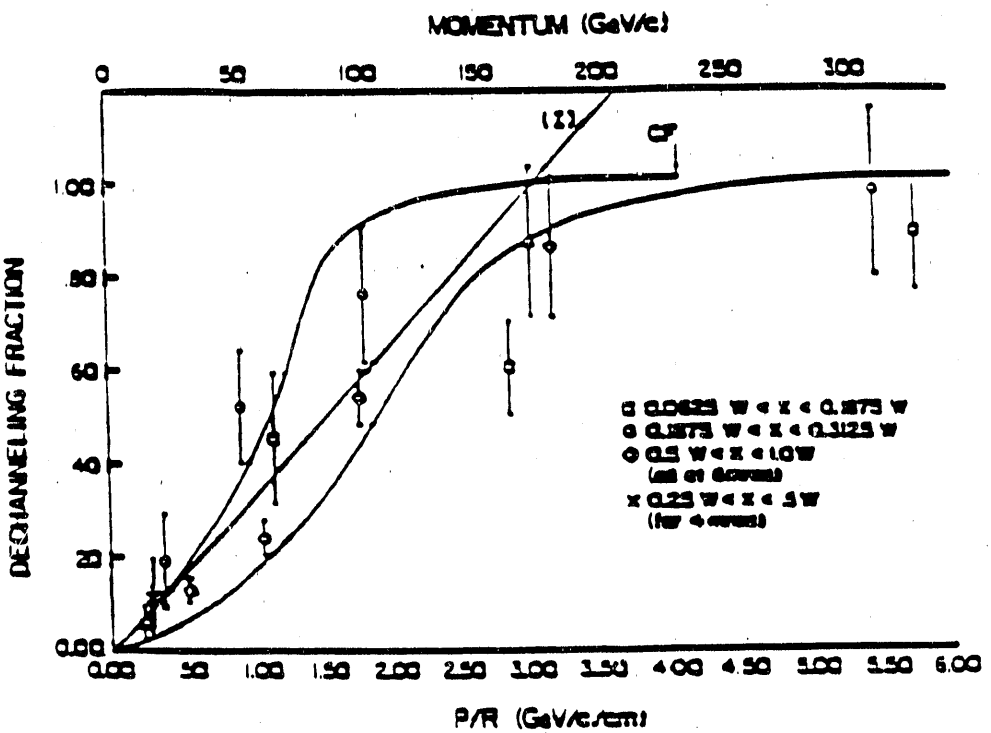

Fig. 7

SFT Silicon Microvertex Detector
Schematic

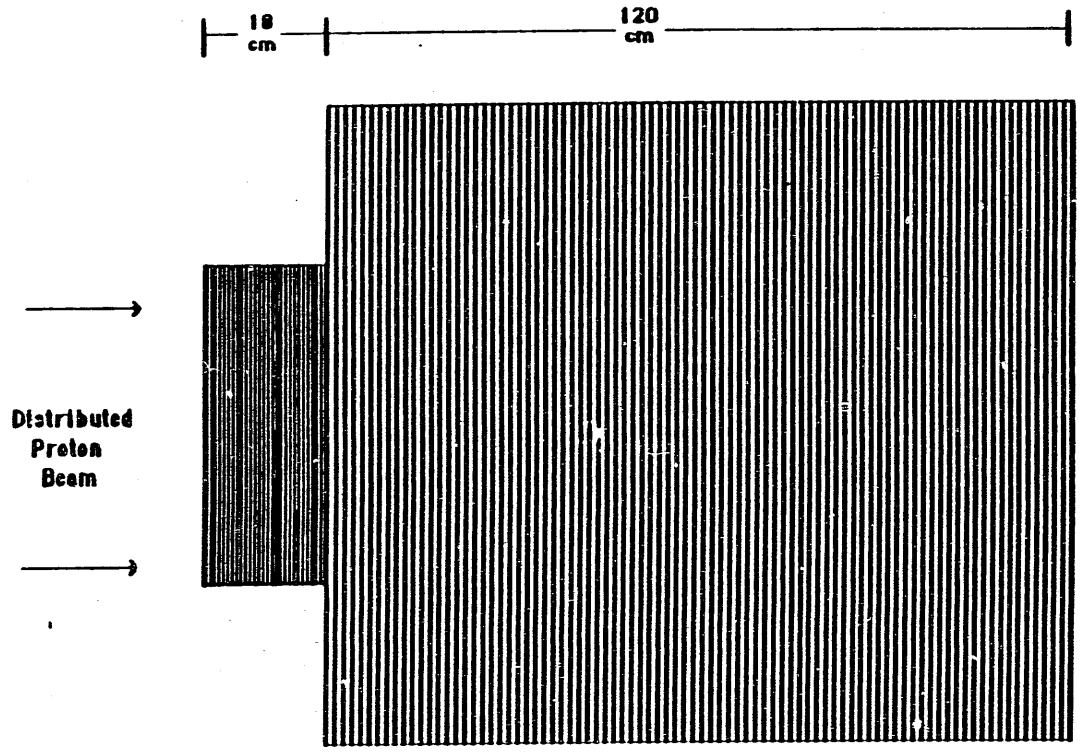

Live Target Section

30 - 200 micron planes
0,30,60 Degree Orientation
10/10/10
6 mm spacing
25 micron pitch
30 Be Foils - 850 micron
0.076 λ 0.137 X_0

Tracking Section

30 - 200 micron planes
0,30,60 Degree Orientation
10/10/10
4 cm spacing
50 micron pitch
0.013 λ_0 0.06 X_0

Fig. 8

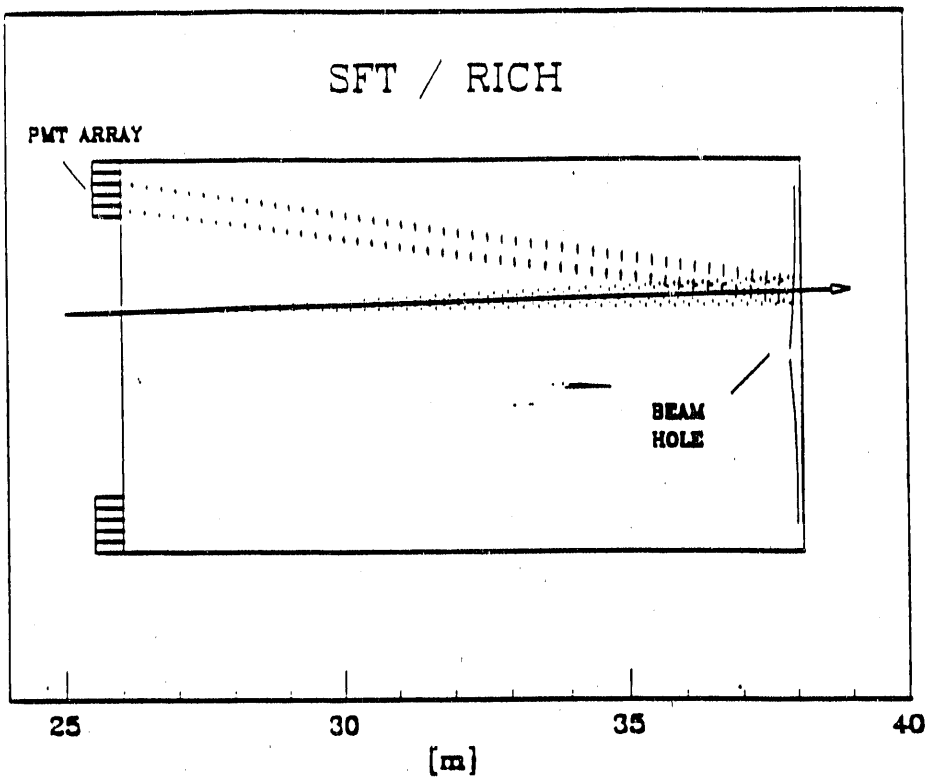

(a)

(b)

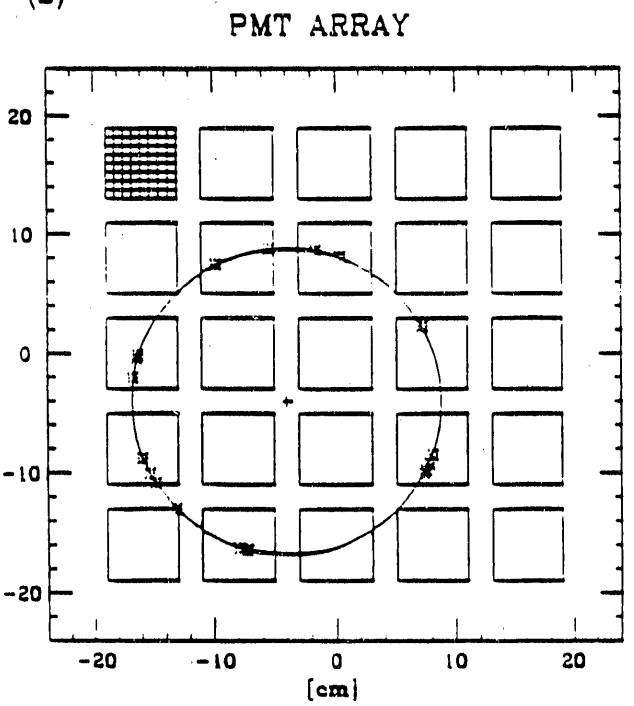

(c)

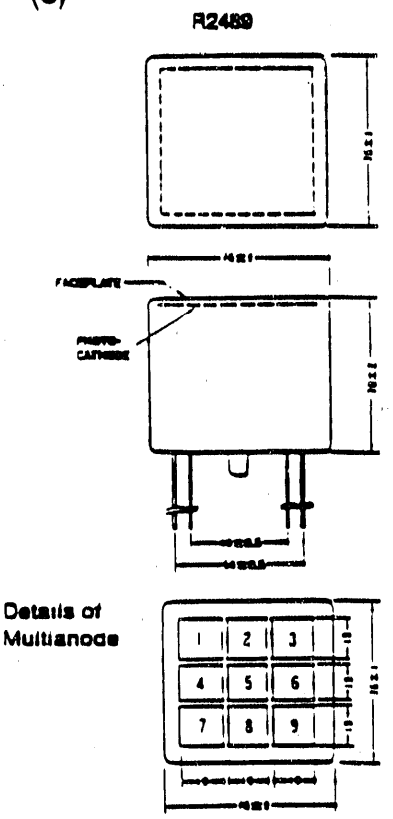

The SFT RICH Detector

Fig. 9

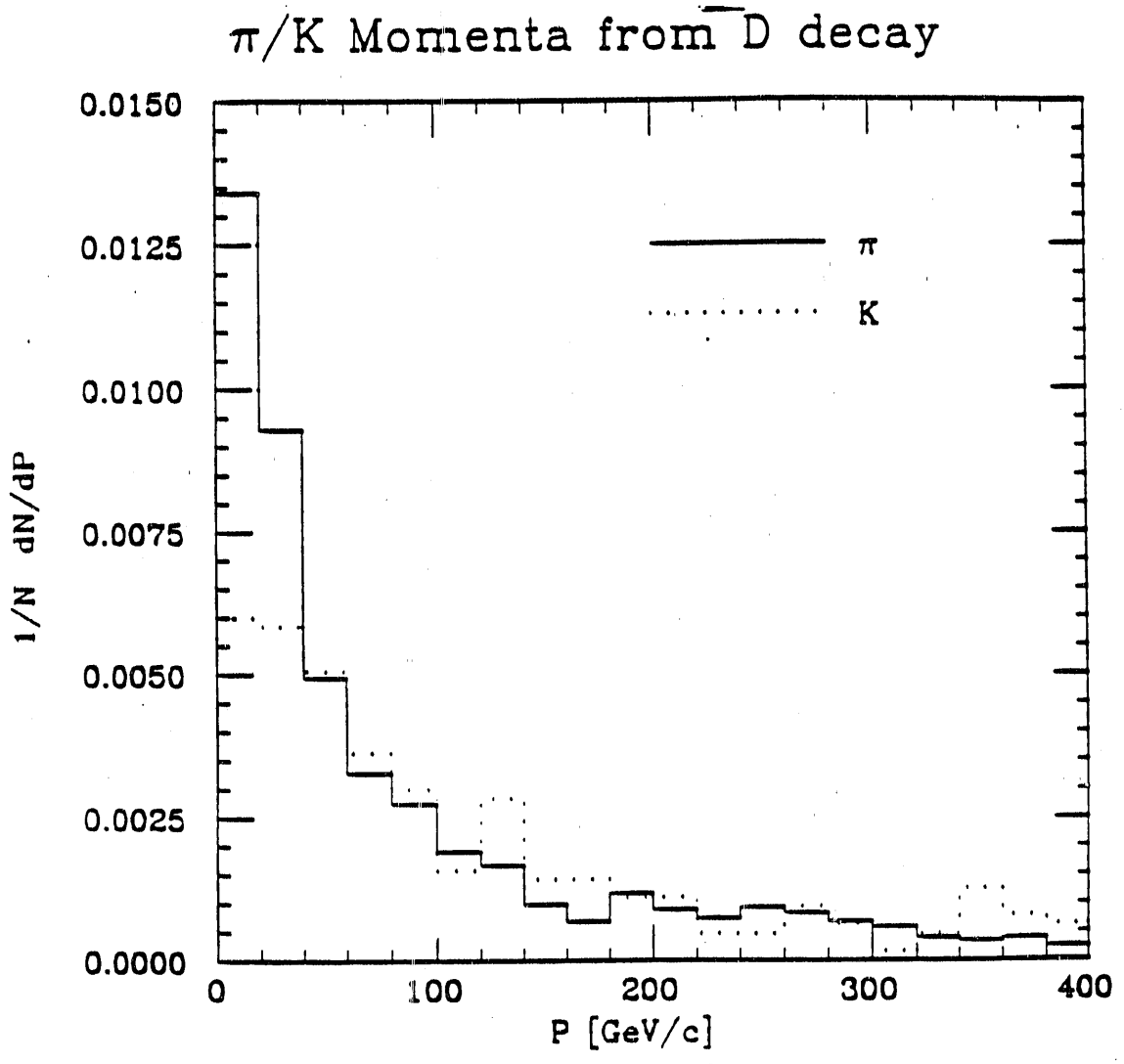
π/K Momenta from D decay
0.0150
0.0125
0.0100
0.0075
0.0050
0.0025
0.0000
1/N dN/dP
π
K
0
100
200
300
400
P [GeV/c]

Fig. 10

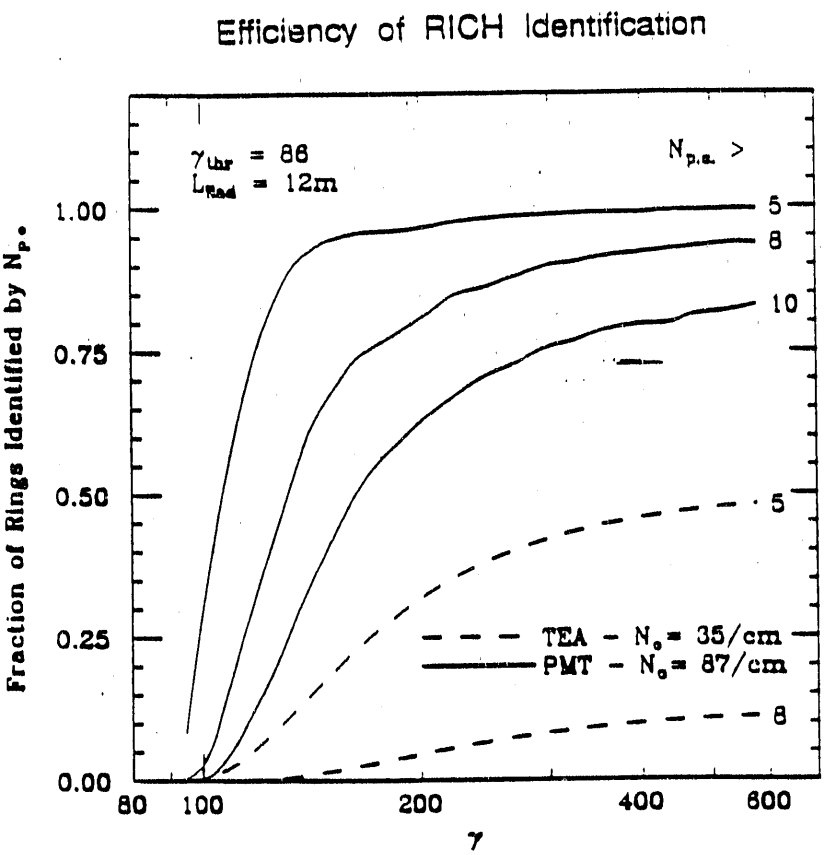
Efficiency of RICH Identification
γ_{thr} = 86
L_{Rad} = 12m
$N_{p.e.}$ >
5
8
10
5
8
TEA - N_0= 35/cm
PMT - N_0= 87/cm
Fraction of Rings Identified by $N_{p.e.}$
1.00
0.75
0.50
0.25
0.00
80
100
200
400
600
γ

Fig. 11

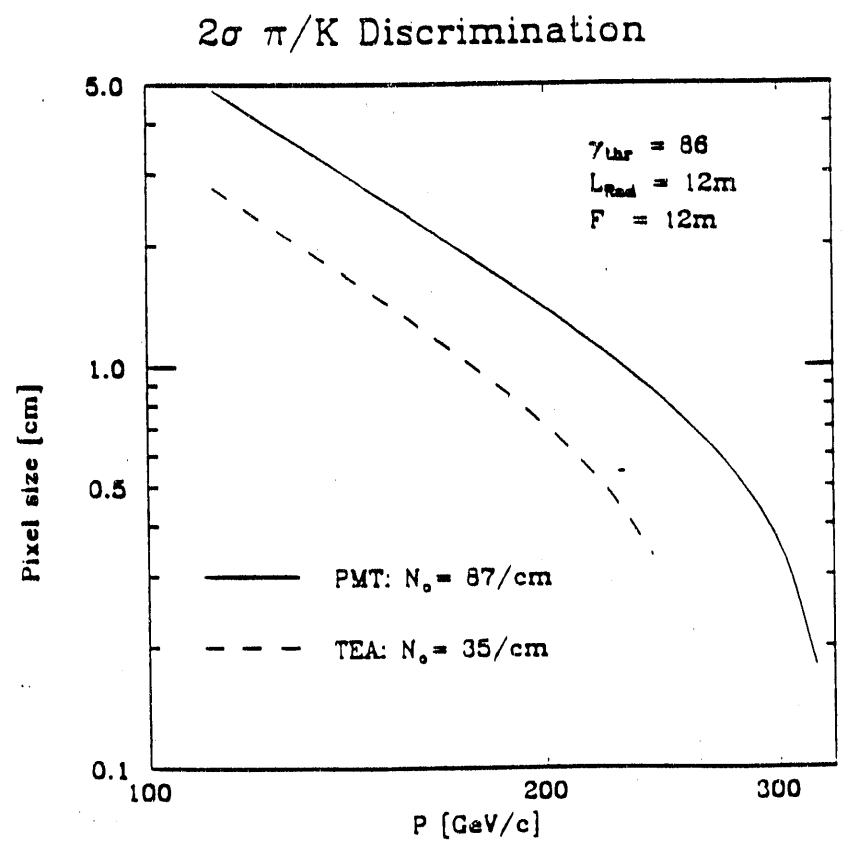
2σ π/K Discrimination
γ_{thr} = 86
L_{Rad} = 12m
F = 12m
PMT: N_0= 87/cm
TEA: N_0= 35/cm
Pixel size [cm]
5.0
1.0
0.5
0.1
100
200
300
P [GeV/c]

Fig. 12

SFT - Electromagnetic Calorimeter

Maximum Electromagnetic Radiation Dose (Mrad)

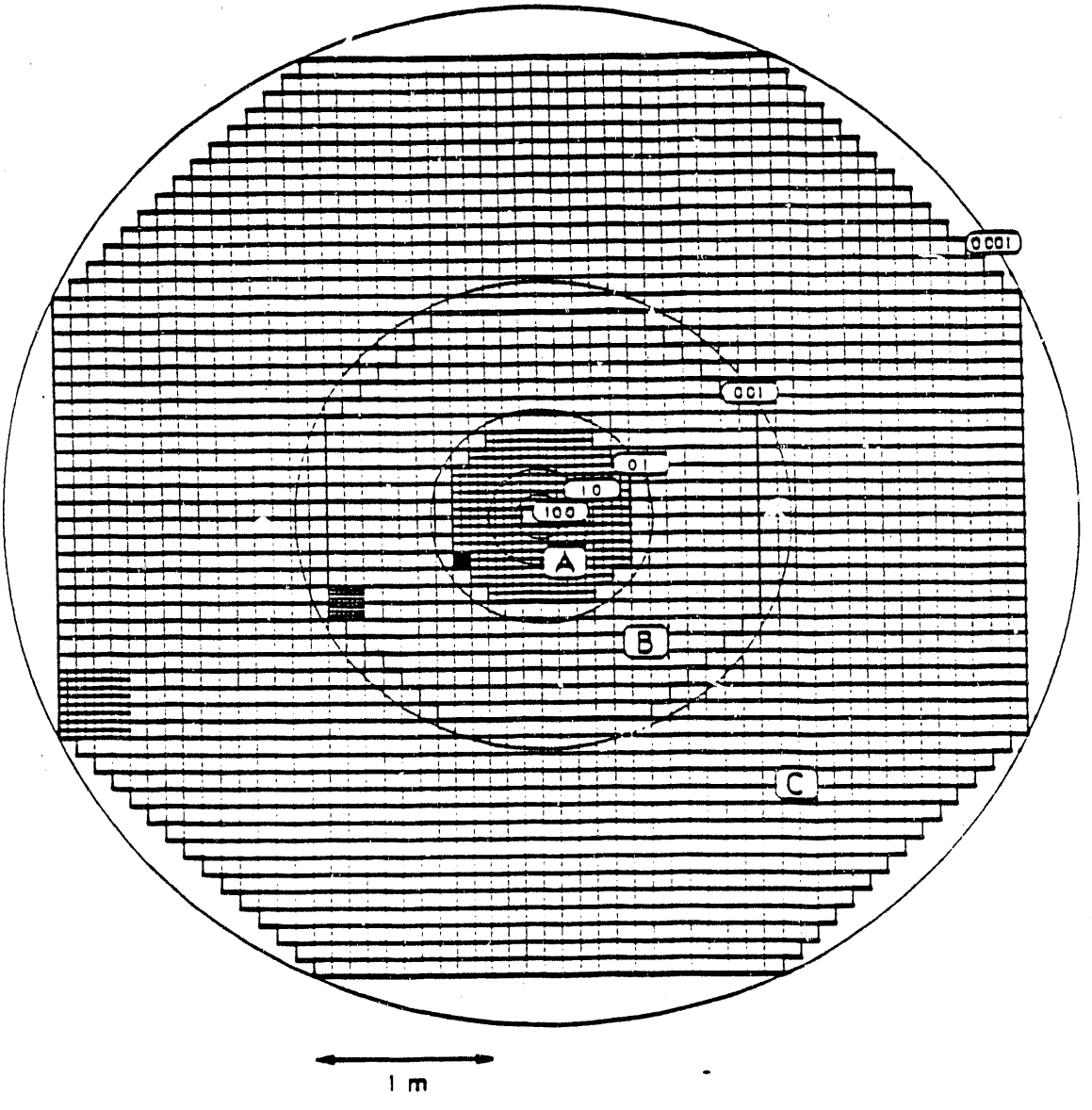

Fig. 13

SFT Inner Calorimeter SCIFI Module

50mm x 50mm Area
16 pixel readout
(all units mm)

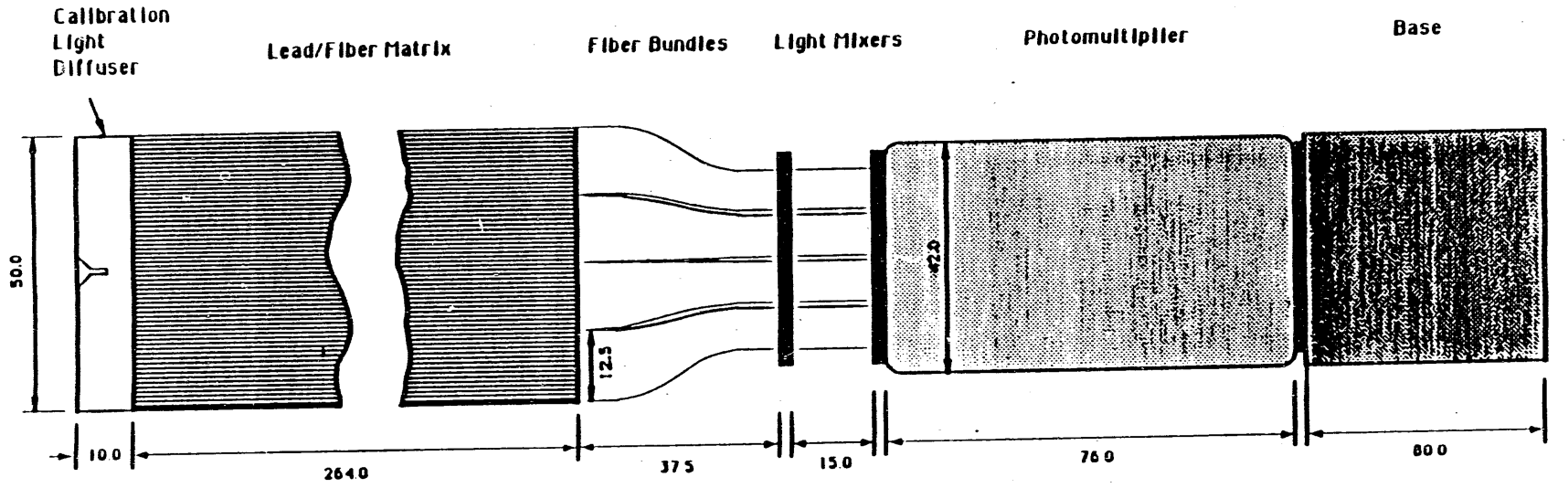

Fig. 14

Photon Energy from $\sqrt{s}$ = 193 GeV Interactions

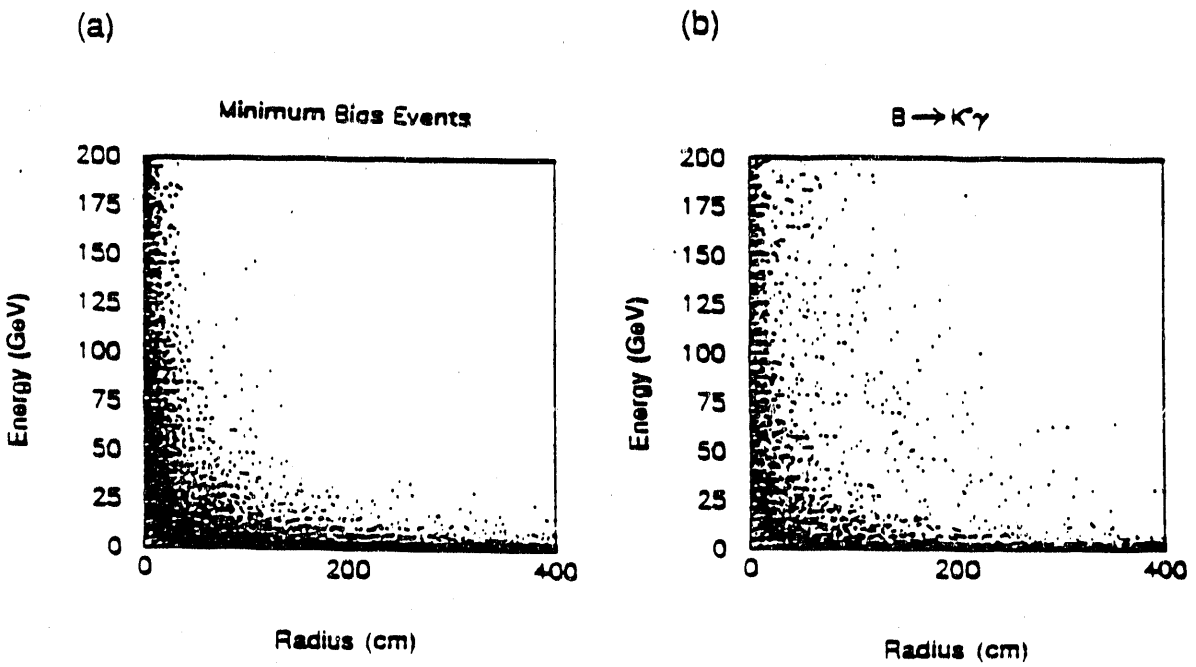

Fig. 15

Resistive Plate Counters

(a)

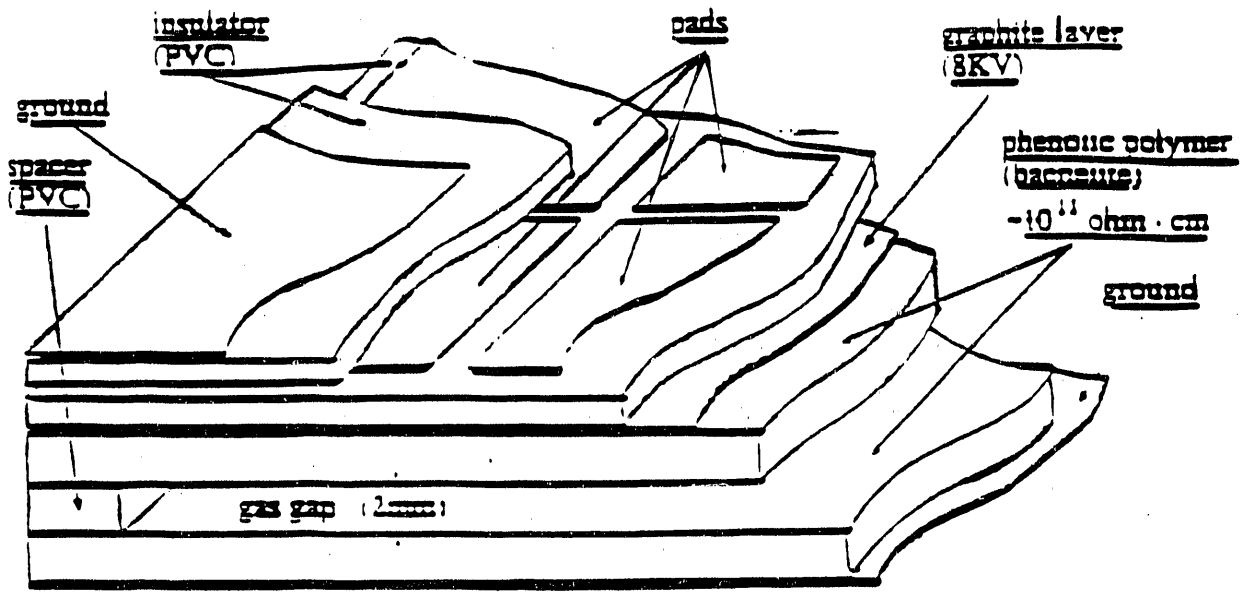

(b) **Resistive Plate Chamber Rate Dependence**

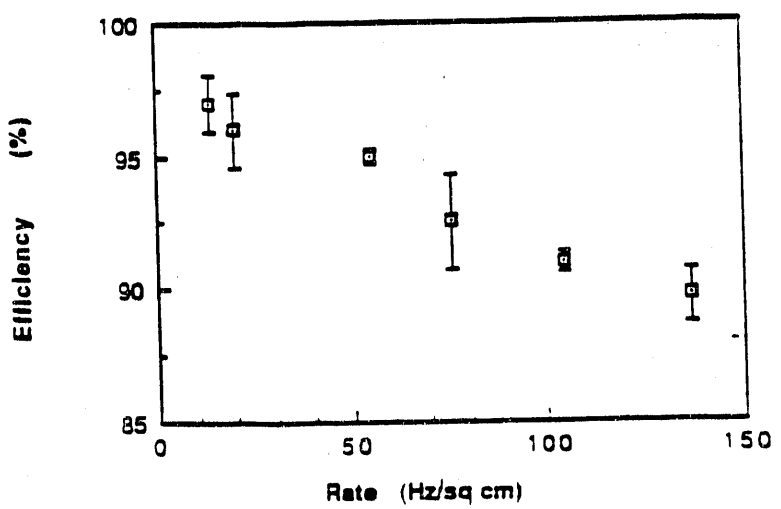

(c) **Typical Pulse Shape**

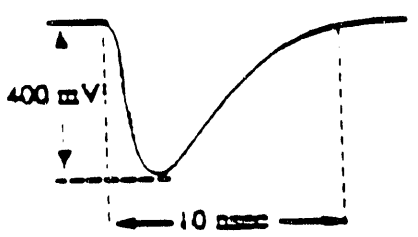

Fig. 16

Momentum of Decay Muons

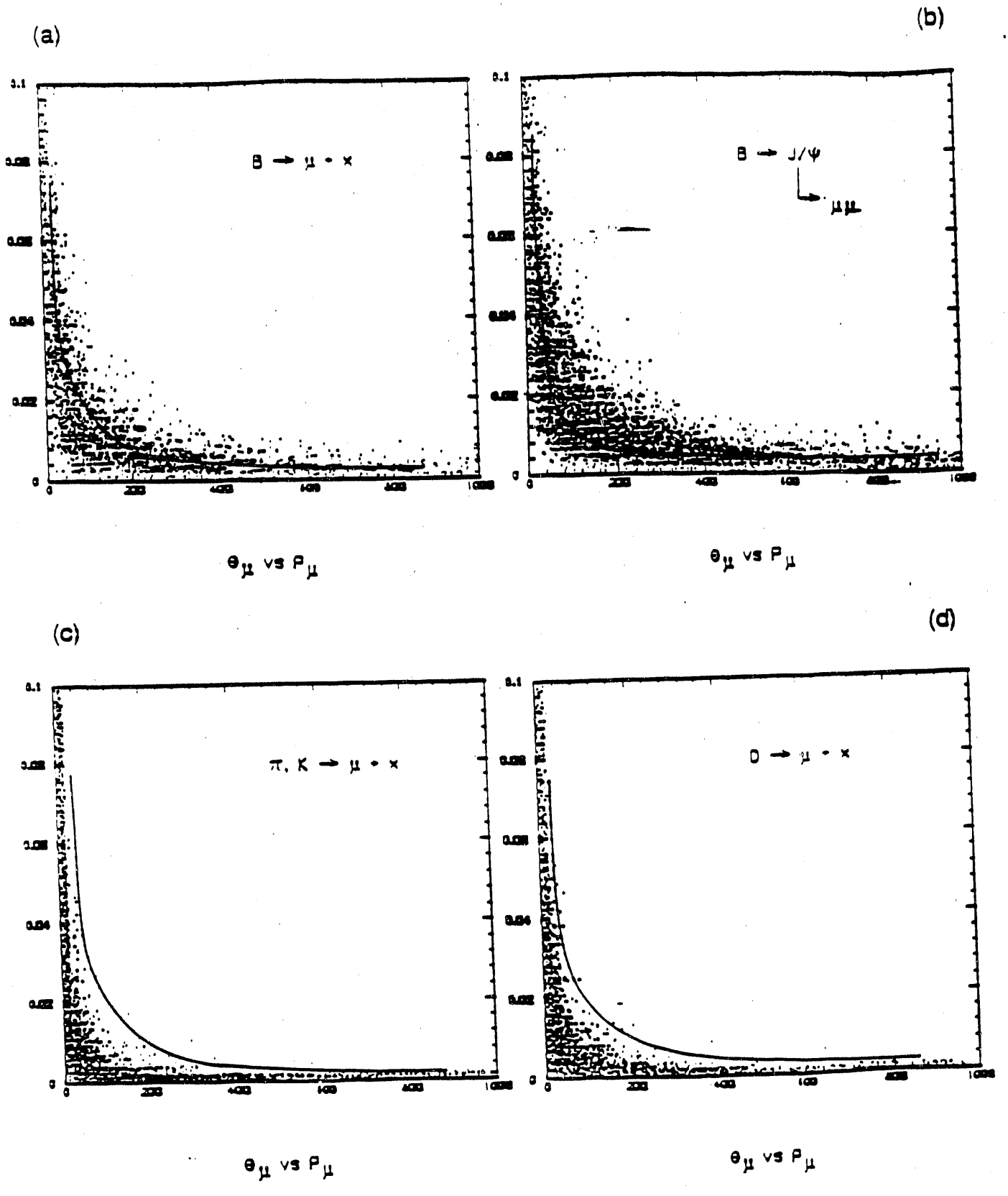

Fig. 17

Muon Trigger Coincidence Scheme

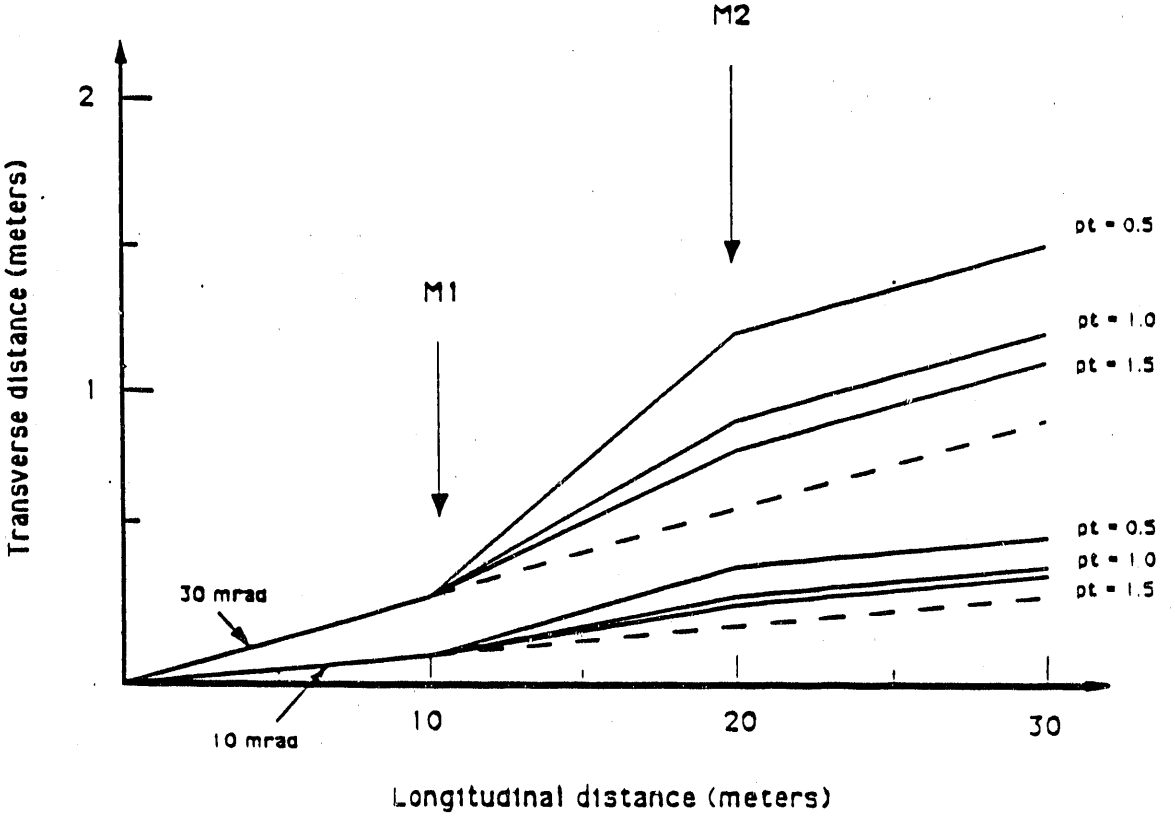

Fig. 18

END

DATE FILMED

02/22/91